catalysts

MDPI

Review

Insights into the TiO_2-Based Photocatalytic Systems and Their Mechanisms

Mohan Sakar [1,2], Ravikumar Mithun Prakash [2] and Trong-On Do [1,*]

[1] Department of Chemical Engineering, Laval University, Quebec, QC G1V 0A8, Canada
[2] Centre for Nano and Material Sciences, Jain University, Bangalore 562 112, India
* Correspondence: Trong-On.Do@gch.ulaval.ca

Received: 22 July 2019; Accepted: 7 August 2019; Published: 9 August 2019

Abstract: Photocatalysis is a multifunctional phenomenon that can be employed for energy applications such as H_2 production, CO_2 reduction into fuels, and environmental applications such as pollutant degradations, antibacterial disinfection, etc. In this direction, it is not an exaggerated fact that TiO_2 is blooming in the field of photocatalysis, which is largely explored for various photocatalytic applications. The deeper understanding of TiO_2 photocatalysis has led to the design of new photocatalytic materials with multiple functionalities. Accordingly, this paper exclusively reviews the recent developments in the modification of TiO_2 photocatalyst towards the understanding of its photocatalytic mechanisms. These modifications generally involve the physical and chemical changes in TiO_2 such as anisotropic structuring and integration with other metal oxides, plasmonic materials, carbon-based materials, etc. Such modifications essentially lead to the changes in the energy structure of TiO_2 that largely boosts up the photocatalytic process via enhancing the band structure alignments, visible light absorption, carrier separation, and transportation in the system. For instance, the ability to align the band structure in TiO_2 makes it suitable for multiple photocatalytic processes such as degradation of various pollutants, H_2 production, CO_2 conversion, etc. For these reasons, TiO_2 can be realized as a prototypical photocatalyst, which paves ways to develop new photocatalytic materials in the field. In this context, this review paper sheds light into the emerging trends in TiO_2 in terms of its modifications towards multifunctional photocatalytic applications.

Keywords: TiO_2; semiconductors; photocatalysis; redox reactions; band gap engineering; nanostructures

1. Introduction

Since the observation of an enhanced electrolysis of water (H_2O) molecules into H_2 and O_2 using TiO_2 as photo-anode and Pt as cathode under UV light irradiation, [1] the research on TiO_2 is gaining significant momentum towards its 'photocatalytic' process, which is coined later on. In 1977, Schrauzer and Guth reported the Pt/Rh metal modified-TiO_2 powders for the photocatalytic splitting of water molecules [2]. Followed by such pioneering work in the field, a range of semiconducting materials have been explored for the photocatalytic properties towards various photocatalytic applications [3–12]. Accordingly, there has been prompt progress in developing various photocatalytic systems to convert the chemical energy through water splitting [13–16] into H_2 and O_2 and other associated reactions [17,18]. Specifically, diverse binary oxide-based photocatalysts have been developed and demonstrated as reliable photocatalysts [19–21].

Despite the emergence of various binary oxide photocatalytic systems, TiO_2 is considered as the most promising material due to its unprecedented stability, excellent physiochemical properties with ease of synthesis, availability, and relatively lower cost [22–24]. In addition to this, TiO_2 exhibits three polymorphs, namely anatase, rutile, and brookite [25], in which the anatase phase is widely used

because of its photocatalytic efficiency as its conduction band has been positioned in the appropriate negative potential, which is the favorable band edge position for redox reactions [26]. Despite such merits and reliable properties, TiO_2 lacks in some of the other specific crucial properties for photocatalysis, such as wide bang gap energy, rapid charge recombination, insufficient transportation, etc. [27]. To surpass such limitations, TiO_2 has been modified in many different ways through chemical and physical modifications, where the former involves doping, composite formation, defects creation, functionalization, plasmonic sensitization, co-catalyst loading, etc., and the other involves size, morphology, and shape modifications, etc. [28].

In this review, we have essentially focused on the versatile modifications of TiO_2 such as morphology modifications, doped TiO_2, hetero-junctions, Z-scheme, plasmonic, ferroelectric/perovskite, chalcogenides, metal–organic frameworks, carbon-based TiO_2, defective TiO_2, etc. TiO_2 may be the only material that has been used to construct the any given aforementioned photocatalytic systems and investigated for almost all the photocatalytic applications such as dye degradations, pharmaceutical degradations, H_2 evolution, O_2 evolution, CO_2 reduction, heavy metal reduction, N_2 fixation, organic synthesis, antimicrobial disinfection, etc. Unlike other existing reviews, which merely provides TiO_2 modifications such as doping, etc., this review paper gives insights into the modifications of TiO_2 towards developing various photocatalytic systems as a whole, which can be prototyped using other materials.

2. Mechanics of TiO_2 Photocatalysis

Photocatalysis (PC) is the process of performing a chemical reaction in the presence of light and a photoactive catalyst, where the charge carriers (electron hole) get separated by the incident photons with sufficient energy and transferred to the respective bands and involved in the redox reactions. The following equations show the reaction mechanism of the photocatalytic process [29,30].

$$\text{Incident photon: Photocatalyst} + h\upsilon \rightarrow e^- + h^+ \quad (1)$$

$$\text{Reduction: } 2H^+ + 2e^- \rightarrow H_2 \; \Delta E = 0 \text{ V} \quad (2)$$

$$\text{Oxidation: } 2H_2O + 4h^+ \rightarrow O_2 + 4H^+ \; \Delta E = 1.23 \text{ V} \quad (3)$$

$$\text{Overall: } 2H_2O \rightarrow 2H_2 + O_2 \; (\Delta G = +237.2 \text{ kJmol}^{-1}) \quad (4)$$

As mentioned in the reaction equations, the incident photons generate the photo-induced electron hole (e^-/h^+) pairs in the semiconductor and the electron involved in the reduction reactions, while the holes are involved in the oxidation reactions. The first and foremost prerequisite for a photocatalyst is to have an appropriate band edge potential (valence band/VB, conduction band/CB) to induce the required redox species. Considering the PC process in TiO_2, the VB and CB level of TiO_2 lies at +2.9 and −0.3 eV, respectively, which leads to the band gap energy of 3.2 eV. It should be noted that the VB and CB level of TiO_2 lies at more positive and more negative values in comparison with the standard redox potential of O_2/H_2O (1.23 eV) and $H+/H_2$ (0 eV) vs. normal hydrogen electrode (NHE), which is one of the more favorable conditions for the photocatalytic redox reactions [31,32].

Apart from the band edge positions, the photocatalytic process also requires enhanced surface reactivity, charge separation, and transportations mechanisms [33]. Upon excitation, the photocatalyst should facilitate the transportation of electrons to the surface, which essentially determines the surface chemistry and reactivity of the photocatalyst. The surface of TiO_2 typically contains more defects, which are often found to be oxygen vacancies; the unpaired electrons in such defects are transferred to the conduction band of TiO_2 and facilitate the catalytic reactions in the system [34]. Interestingly, the accumulation of electrons leads to the band bending phenomenon in TiO_2 that considerably redesigns the transportation of charges or energy to the surrounding molecules [35]. Charge recombination dynamics is one of the serious issues in a photocatalyst. Regarding TiO_2, with its indirect band gap, it is proposed that the recombination process occurs via non-radiative pathways and, thus, the lifetime

of charge carriers in TiO_2 varies from picoseconds to milliseconds [36,37]. In addition, the observed relatively enhanced PC efficiency of TiO_2 can also be ascribed to its electron and hole trapping [38]. Generally, the photo-induced charge carriers do not tend to recombine directly due to the factors such as carrier trapping, band bending, etc. Accordingly, it is predicted that the holes in TiO_2 can be trapped either at the "bridging" O^{2-} or "surface bound" OH^- anions, which results in the generation of $O^{-\bullet}$ and/or $OH^\bullet$ centers, respectively. Similarly, the photo-induced electrons can be forced to migrate into the bulk from surface, where they can be delocalized in possible Ti sites. Furthermore, it is also predicted that in TiO_2 it is of more possible for bulk trapping rather than surface trapping and thereby TiO_2 shows relatively enhanced photocatalytic activities as compared to the other semiconducting oxide-based photocatalysts [38–40].

3. Versatile Modifications of TiO_2 and Their Photocatalytic Mechanisms

TiO_2 as a photocatalyst has been modified in a variety of ways that generally includes (i) morphological, (ii) defective, (iii) elemental doping (cationic/anionic), (iv) plasmonic metal-loading, composites with (v) binary oxides, (vi) perovskite systems, (vii) metal–organic frameworks, (viii) carbon materials, (ix) chalcogenides, etc. These modifications essentially lead to development of new photocatalytic systems, enhancing (i) the overall visible light/full-sunlight absorption, (ii) charge separation, (iii) recombination resistance, (iv) charge transportations, and (v) tuning of the band edge potential of the system. Accordingly, the following section presents some of the recent studies that mainly highlight the photocatalytic mechanism/functions in such chemically and physically modified TiO_2.

3.1. Morphology-Dependent Photocatalytic Properties of TiO_2

Photocatalysis can be influenced by the size, shape, and morphology of the photocatalyst due to the spatial confinements of electrons in the system [41,42]. For instance, compared to bulk, the surface reactivity is higher for the nanoparticles, where their high surface area/energy facilitates the enhanced (i) catalytic activity on the surface, (ii) surface adsorption of the molecules, and (iii) promotion of charge carriers to surface. The size parameter also considerably influences the band-gap energy as well as band-edge position in a photocatalyst. Similarly, the geometrics of photocatalyst also influences the PC process. For instance, compared to the particles, the one-dimensional nanostructures show improved activity due to the enhanced "delocalization of electrons" in the conduction band of the photocatalyst [43,44]. Further, photocatalysts also demonstrate the crystal-facet-dependent efficiencies towards various photocatalytic applications. TiO_2 nanocrystals with different shapes, as shown in Figure 1a–f, have been synthesized and demonstrated for photo-reforming of methanol into hydrogen under UV light [45].

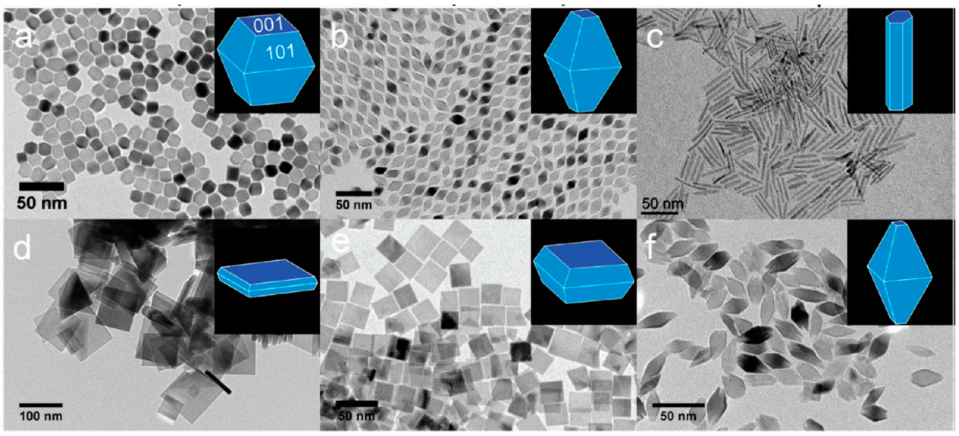

Figure 1. TEM images of TiO_2 NCs synthesized using the precursor TiF_4 (**a**,**d**), a mixed precursor of TiF_4 and $TiCl_4$ (**b**,**e**), and $TiCl_4$ (**c**,**f**). Those depicted in a−c and d−f are synthesized in the presence of OLAM and 1-ODOL, respectively. (reproduced with permission from ref. [45]).

In another study, the synthesis of TiO_2 solid and hollow nanocubes have been demonstrated, as shown in Figure 2, and applied for the photocatalytic-mediated synthesis of benzimidazole under UV and visible conditions [46]. Similarly, TiO_2 with different morphologies such as nanospheres, nanocubes, nanotubes, nanorods, nanoflowers, nanosheets, and nanofibers have been synthesized and studied for their photocatalytic applications [47–53]. The size and morphology control over TiO_2 photocatalyst exhibit significant influences over their (i) optical properties such as tunable band-gap energy, repositioning of band edge positions, visible light absorption, etc., (ii) electronic properties such as increased carrier lifetime, enhanced photocurrent conduction, reduced recombination, and (iii) surface properties such as enhanced surface energy, porous structures, enhanced surface adsorption, etc. Realizing the photocatalytic phenomenon, these properties are very much important to achieve the enhanced efficiencies in the photocatalytic materials.

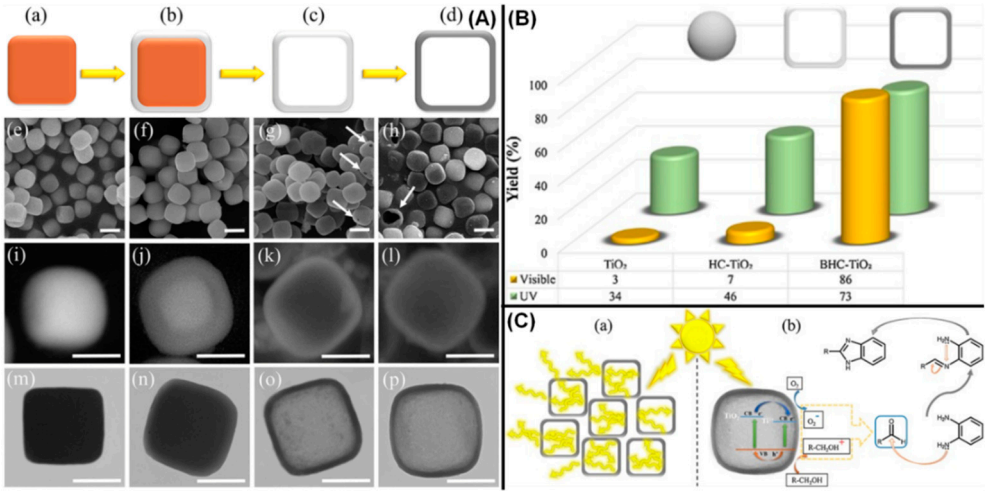

Figure 2. (**A**) Overall flowchart for fabrication of black hollow nanocubic (BHC)-TiO_2 (**a**–**p**), (**B**) Comparison photocatalytic activity of different TiO_2 nanostructures in the synthesis of benzimidazole under UV and visible conditions; (**C**) Schematic diagram of the light scattering effect caused by BHC-TiO_2 nanocubes (**a**) and schematic of the proposed mechanism for benzimidazole preparation by BHC-TiO_2 architecture (**b**) (reproduced with permission from ref. [46]).

3.2. Doped TiO_2

Doping can be essentially classified into two categories, (i) cationic and (ii) anionic doping. Accordingly, TiO_2 has been widely modified through doping under both categories. The cationic and anionic doping in TiO_2 leads to the formation of new energy levels underneath the conduction band and above the valence band [54]. The former doping has often been found to reduce the band gap energy and facilitates the visible light absorption and charge separation in TiO_2, whereas the latter often helps in shifting of the VB position, mitigates the defects, and enhances the chemical stability of TiO_2 [55]. The anionic dopants such as N, C, S, and P have been largely doped in TiO_2. Among them, the N doping showed relatively enhanced photocatalytic activity due to the increased stability in the system. Similarly, there are variety of elements doped at the cationic site of TiO_2 and explored for their photocatalytic activities under UV-visible light.

3.2.1. Anionic Doping inTiO_2

Chen et al. reported the origin of visible-light absorption characteristics of C-, N-, and S-doped TiO_2 nanomaterials [56]. In their studies, the TiO_2-P25 showed the typical band-edge absorption around 390 nm with band gap energy of 3.2 eV, while the C and S doping also showed the same values, however the N-doping showed an absorption around 415 nm with band gap energy of 3.0 eV. Further, their valence band-X ray photoelectron spectra revealed an interesting feature that the doping of C, S,

and N created additional states in the TiO_2 system, as shown in Figure 3A [56]. These additional states were attributed to the C 2p, S 3p, and N 2p orbitals and they were found to add deeper states into the band gap of TiO_2 in the order of C > N > S. Emy et al. reported the band gap engineering in the anionic co-doped TiO_2 [57]. According to their investigations, they have explained that in F-doped TiO_2, the band gap reduction is mediated by the presence of surface Ti^{3+} defects underneath the CB, while in N-doped TiO_2, the mid-band states have been formed as the N species fill voids as impurities above the VB. On the other hand, the co-doping of N and F into TiO_2 leads to the biggest band gap reduction to 2.24 eV from 3.19 eV, where it is attributed to the doping induced creation of defects and shifting of the VB tail towards Fermi level as shown in Figure 3B [57].

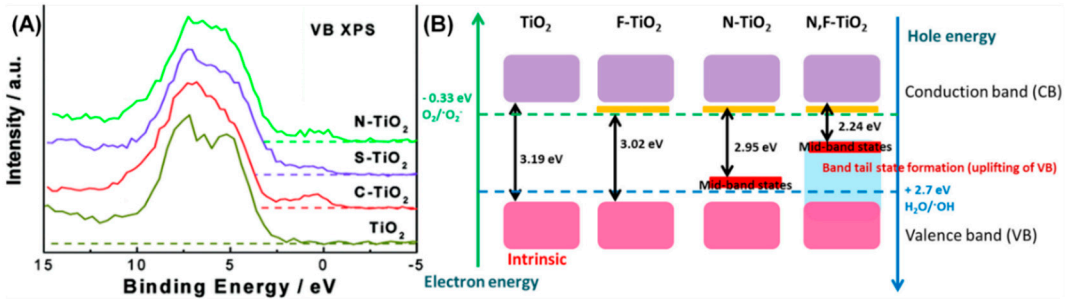

Figure 3. (**A**) Valence band (VB) XPS spectra of pure and (C, S, N)-doped TiO_2; (**B**) proposed band gap engineering structure for all (F, N) doped TiO_2 (reproduced with permission from refs. [56,57], respectively).

Based on the available experimental evidences and theoretical results obtained by Wang et al. [58], we have concluded that both the bang gap narrowing and the overlapping of O 2p state with the dopant-induced states strongly affect the photocatalytic activities of anion-doped TiO_2. However, Kuznetsov et al. [59] have reported that the visible light absorption happening in these doped-TiO_2 may be due to the formation of color centers and may not be due to the band gap narrowing. Further, they have also argued that the red shift in the absorption edge could be due to the emergence of color centers and the doping (heavily) may completely lead to the formation of material with completely different chemical composition from TiO_2 with different electronic band structures. However, it should be noted that the anion-doped TiO_2 is considered as the second-generation photocatalysts [60].

3.2.2. Cationic Doping in TiO_2

As described, the cationic doping essentially introduces the intra-band energy levels close to the CB of TiO_2, which leads to the red shift in the optical property of the system and it is also observed in various cations such as transition metal, [61–63], rare-earth [64–66], and other metals [67–69] doped TiO_2. However, the main drawback of the cation doping is the creation of more trapping sites for charge carriers (both electrons and holes) that considerably reduces the efficiency of the photocatalyst. This is because the trapped carriers tend to recombine with the respective mobile carriers in the system. The mechanism of cation doping is essentially to tune the Fermi level and electronic structure of *d*-electron configuration in TiO_2, thereby to tune the energy levels to absorb the visible light energy and to enhance the overall photocatalytic efficiency of the system as shown in Figure 4a–c [70–72].

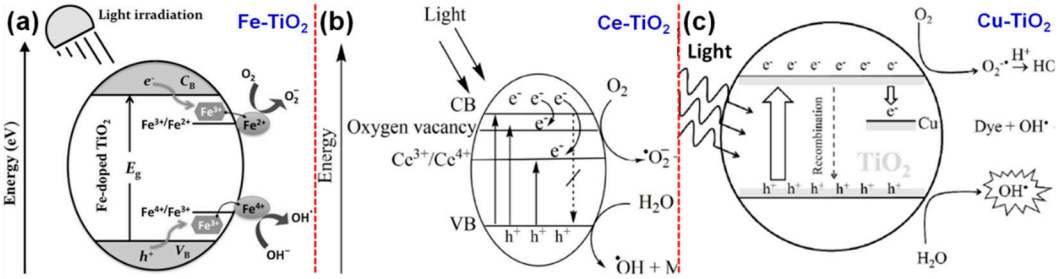

Figure 4. Band gap engineering in TiO_2 via (**a**) Fe, (**b**) Ce, (**c**) Cu doping, showing the formation of dopant energy states underneath the conduction band of TiO_2 and associated carrier dynamics (reproduced with permission from refs. [70–72], respectively).

Consequently, there have been many cations doped in TiO_2 towards enhancing its PC activities. In such cation doping, TiO_2 has been doped with the (i) transition metals such as Sc, V, Cr, Mn, Fe, Co, Ni, Cu, Zn, Y, Zr, Nb, Mo, Cd, and W [73–84]; (ii) rare-earth metals such as Ce, Pr, Nd, Sm, Eu, Gd, Tb, Dy, Er, Yb, and La [85–89]; and (iii) other metals such as Li, Mg, Ca, Se, Sr, Al, Sn, and Bi [90–97]. In the case of rare earth elements doping, the electronic configurations such as 4f, 5d, and 6s are found to be favorable to tune the band edge positions, density of states, and width of VB and CB via altering the crystal, electronic, and optical structures in TiO_2 [98–100]. In addition, the rare earth elements tend to form complexes through their *f*-orbital and form various Lewis-based organic compounds, thereby improving the photocatalytic activities of TiO_2 [101,102]. For instance, lanthanum (La) leads to the NIR absorption in TiO_2 [103], cerium (Ce) owing to its tunable electronic configuration of 4f states, such as $4f^0 5d^0$ (Ce^{4+}) and $4f^5 d^0$ (Ce^{3+}), where it leads to the formation of mid-band gap in TiO_2 that facilitates the absorption of in the visible region 400–500 nm [104,105].

3.3. Hetero-Junction TiO_2

Coupling of TiO_2 with other semiconductors, especially narrow band gap semiconductors to form a heterojunction, is considered to be one of the promising strategies to improve the photocatalytic efficiencies of the system [106,107]. The selection of semiconductors towards forming the heterojunction should be made in such a way that they have different band edge potential and conducting types. For instance, Figure 5a,b depicts the charge transfer mechanisms in the p-n and non p-n junctions between the semiconductors [107]. Such configuration provides several features to the system, such as it helps improve the (i) charge separation, (ii) life time of the charge carriers, (iii) recombination resistance, and (iv) interfacial charge transportations towards the adsorbed molecules [106,107]. The semiconductor that coupled with the host-semiconductor would typically act as a sensitizer. In such cases, it is the sensitizers that get excited and transfer/inject the carriers into the host-semiconductor and, therefore, the VB of the sensitizer should be more cathodic than the VB of TiO_2, so that the holes cannot migrate to the TiO_2; thereby, the charge separation remains in the system [108]. These kinetics facilitate the phenomenon of electron injections into TiO_2 as demonstrated in Figure 5c,d [109]. Based on such thermodynamics of heterojunction formations, Bessekhouad et al. developed Cu_2O/TiO_2, Bi_2O_3/TiO_2, and $ZnMn_2O_4/TiO_2$ heterojunctions towards the photocatalytic degradation of multiple organic pollutants Orange II, benzamide, and 4-hydroxybenzoic under UV-visible light [109]. In this study, they have discussed that the CB of Cu_2O is positioned at −1.54 eV, which is more negative than the CB of TiO_2 (−0.41 eV) that favored the transfer of electrons to TiO_2 from Cu_2O. Importantly, such electrons-transfer kinetics led to the faster degradation of Orange II molecules as compared to benzamide and 4-hydroxybenzoic molecules as they require more holes oxidation. The same results were also observed in the case of Bi_2O_3/TiO_2 heterojunction. In the case of $ZnMn_2O_4/TiO_2$ heterojunction, the CB position of $ZnMn_2O_4$ is estimated to be +0.062 eV, which is greater than the CB of TiO_2. Under such circumstances, the electrons excited to the CB of $ZnMn_2O_4$ could not be transferred to TiO_2, but the opposite would happen when the TiO_2 is excited. However, $ZnMn_2O_4/TiO_2$

heterojunction was not found to be effective and, in fact, it had a tendency to decrease the efficiency of TiO_2. From their results, they finally concluded that the band edge positions of the semiconductors involved should be compatible for an effective inter-particle electron injection to happen in the system and, more importantly, the generated holes must be promoted and react highly at the surface to have an improved carrier separation process.

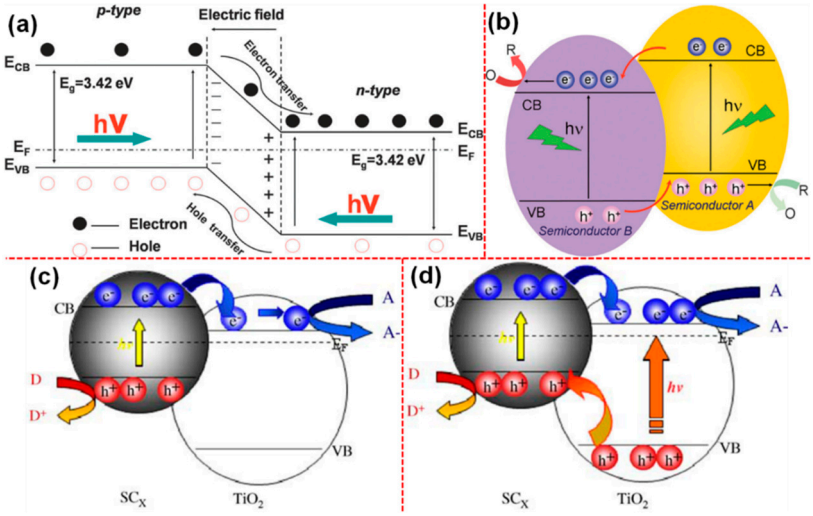

Figure 5. Schematic diagram showing the energy band structure and electron-hole pair separation in the (**a**) p-n heterojunction; (**b**) non p-n heterojunction; (**c**) energy diagram illustrating the coupling of two SC in which vectoral electron transfer occurs from the light-activated SC to the non-activated TiO_2; (**d**) diagram depicting the coupling of SC in which vectoral movement of electrons and holes is possible (reproduced with permission from refs. [107,109]).

As aforementioned, the charge transportation mechanism in heterojunction structure is dependent upon the band-edge levels of the semiconductors forming the heterojunction. For instance, the Fe_3O_4/TiO_2 has been widely studied in this direction. Liu et al. [110] reported the 3D flower-like α-Fe_2O_3@TiO_2 core-shell nanostructures, in which the observed photocatalytic efficiency was attributed to the interfacial charge transportation.

As shown in Figure 6a, where they have irradiated the photocatalyst under UV-visible light, it will excite both the semiconductors. Upon the contact of α-Fe_2O_3 with TiO_2 system, the excited electrons in α-Fe_2O_3 get injected into the CB of TiO_2 due to the relative work function of α-Fe_2O_3 (5.88 eV) and TiO_2 (4.308 eV) system as it leads to the positioning of CB of TiO_2 to be positioned below the CB α-Fe_2O_3. The study by Xia et al. [111] proposed the charge transfer kinetics in α-Fe_2O_3@TiO_2 system under UV and visible light irradiation separately, as shown in Figure 6b. They explained that under visible light irradiation, the carriers get excited in α-Fe_2O_3 and transferred to TiO_2, whereas no excitation would happen in TiO_2 as the system is irradiated by visible light and, subsequently, the charges carrier would be promoted to the surface and perform the photocatalytic redox reaction. On the other hand, it was observed that the system was irradiated under UV light, carriers in TiO_2 get excited, and the α-Fe_2O_3 becomes recombination center of the photo-induced carriers; as a result, α-Fe_2O_3@TiO_2 exhibits relatively poor photocatalytic activity. To address such issues and towards making the α-Fe_2O_3@TiO_2 to work efficiently, Lin et al. [112] developed TiO_2 with abundant oxygen vacancies via self-doping, which greatly shifted the VB edge position to 2.50 eV (vs. NHE), which is very close to that of α-Fe_2O_3 (2.48 eV) and unaltered CB position with respect to the CB position of α-Fe_2O_3, as shown in Figure 6c. However, despite the considerable amount of research that has been done on TiO_2-based heterojunction photocatalyst, the carrier dynamics and their transportation, and thereby the photocatalytic process, should be studied in detail [113,114].

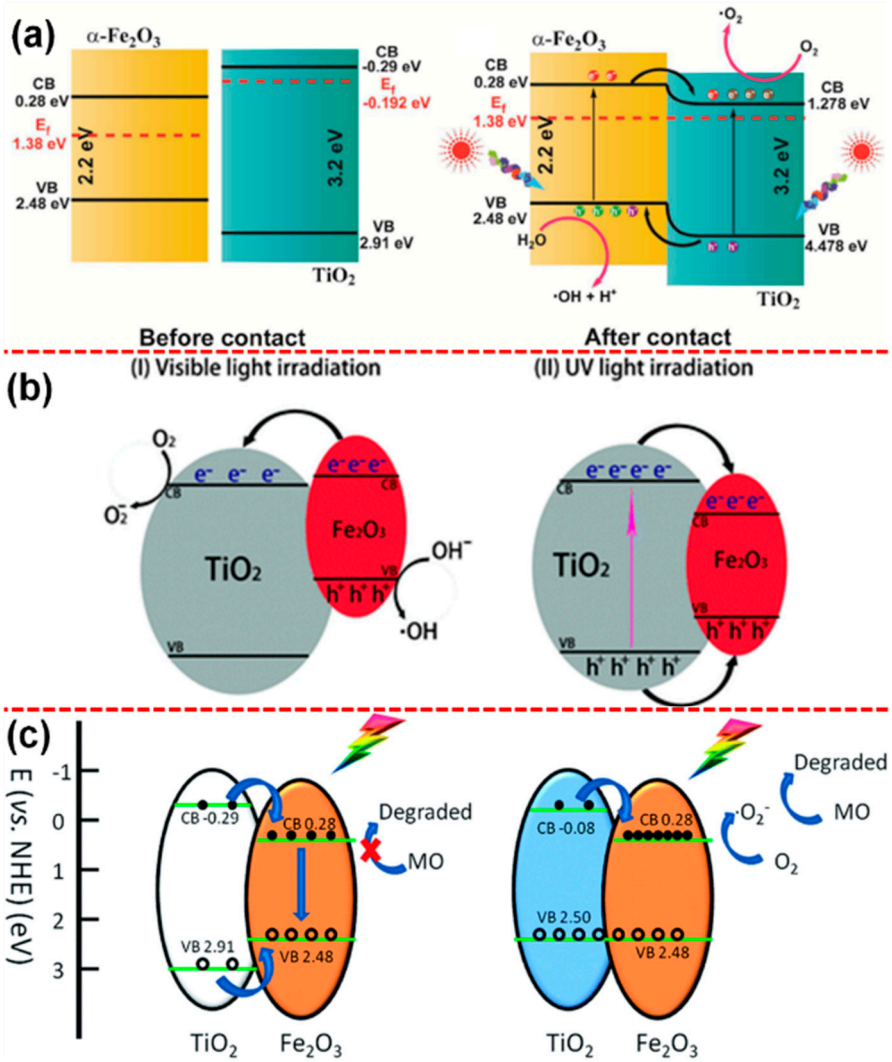

Figure 6. (**a**,**b**) Schematic diagram of the band edge positions and charge transfer mechanism in various α-Fe_2O_3@TiO_2 photocatalytic systems under UV and visible light irradiation. (**c**) The presence of abundant oxygen vacancies in TiO_2 shifts its VB edge position and aligns it to the VB of Fe_2O_3 (reproduced with permission from refs. [110–112], respectively).

3.4. Z-Scheme-Based TiO_2

The concept of Z-scheme photocatalytic process is essentially derived from the natural photosynthesis process, which demonstrated a significantly enhanced potential towards accomplishing high photocatalytic efficiencies [115]. The Z-scheme photocatalyst is typically constructed by coupling two photocatalytic semiconductors, which is likely similar to the conventional heterojunction photocatalyst [116]. However, Z-scheme has a unique mechanism for the injection/transfer of charge carrier into the adjacent semiconductor, as shown in Figure 7a,b [117]. Notably, among the two coupled photocatalysts in Z-scheme, one will be an oxidation and the other will be a reduction photocatalyst. The selection of such oxidation and reduction photocatalyst will be based on the VB and CB edge position, which is dependent upon the specific applications [118]. As a result of such meticulous construction, Z-scheme systems demonstrate exotic features such as (i) simultaneous strong reduction-oxidation abilities, (ii) spatial separation of reduction and oxidation active sites, (iii) enhanced carrier-separation efficiency with high redox abilities, and (iv) extended light absorption range [119,120].

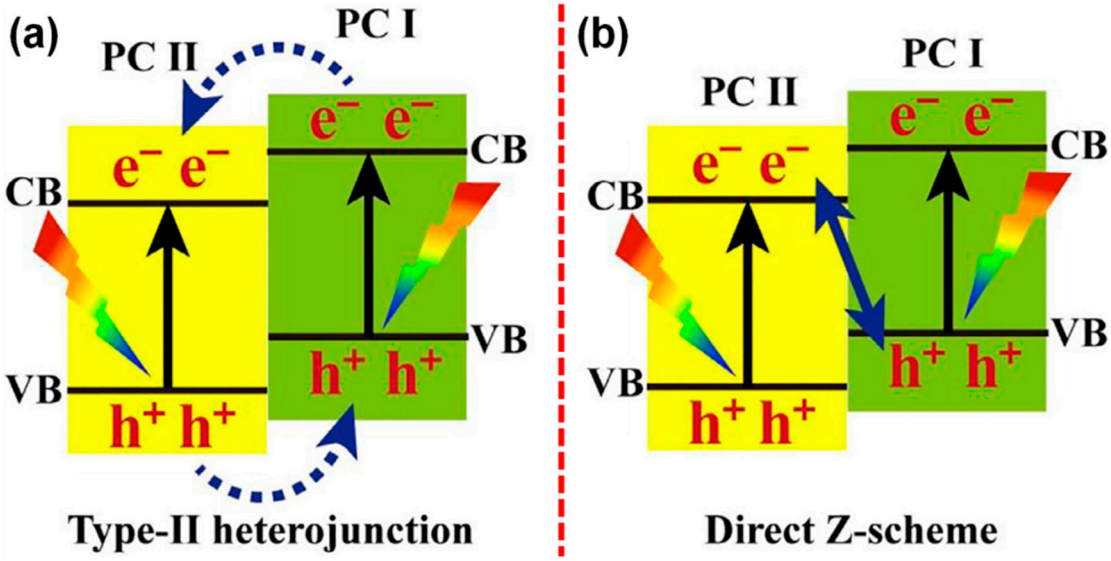

Figure 7. Schematic illustration of the (**a**) typical heterojunction and (**b**) Z-scheme photocatalysts (reproduced with permission from ref. [117]).

In the Z-scheme-based systems, TiO_2 has been largely used as oxidation photocatalyst owing to their low VB position and accordingly, it has been coupled with the other photocatalytic systems such as CdS [121,122], g-C_3N_4 [123–125], NiS [126], $ZnIn_2S_4$ [127], Cu_2O [128], and WO_{3-x} [129] owing to their high CB position that act as the reduction photocatalysts. As shown in Figure 7a [117], in the typical heterojunction photocatalyst, the separated electron holes in PCI will be injected into the respective CB and VB of the PCII. In contrast, the charge transfer mechanism in Z-scheme always follows a signature pathway in which the electrons excited to the CB of low VB photocatalyst will be injected into the VB of the high CB photocatalyst (Figure 7b) [117]. As listed above, Figure 8a–d shows the mechanism of various TiO_2-based Z-scheme photocatalysts. Interestingly, Fu et al. [128] proposed a Z-scheme system mediated by Ag located at the interface of the TiO_2 and Cu_2O. They observed that the TiO_2 and Cu_2O coupled photocatalyst demonstrated a relatively poor photocatalytic performance; as a result, they proposed that upon the irradiation of TiO_2 and Cu_2O, the electrons in the CB of Cu_2O get transferred into the TiO_2 and meanwhile, the holes in VB of TiO_2 get transferred to Cu_2O. Such a process essentially led to the depletion of hole density in the VB of TiO_2 and it increased in the VB of Cu_2O. Under such circumstances, due to the low positive VB edge position of Cu_2O, it has insufficient energy to oxidize the OH or H_2O molecules. To address such an issue, they introduced Ag into the interfacial contact of TiO_2 and Cu_2O, as shown in Figure 8e [128].

In this TiO_2–Ag–Cu_2O system, firstly, the equilibrium in Fermi levels has been established; thereby, upon irradiation, the excited electrons in the TiO_2 CB get injected into Ag and due to the localized electric field created by Ag, these electrons are further injected into the Cu_2O and enhanced the photocatalytic efficiency of the system. Further, they proposed that this system keeps the photo-induced holes on more positive potential (VB of TiO_2) and electrons on more negative (CB of Cu_2O), which essentially enhance the redox ability as well as the charge separation efficiencies of the system as a whole.

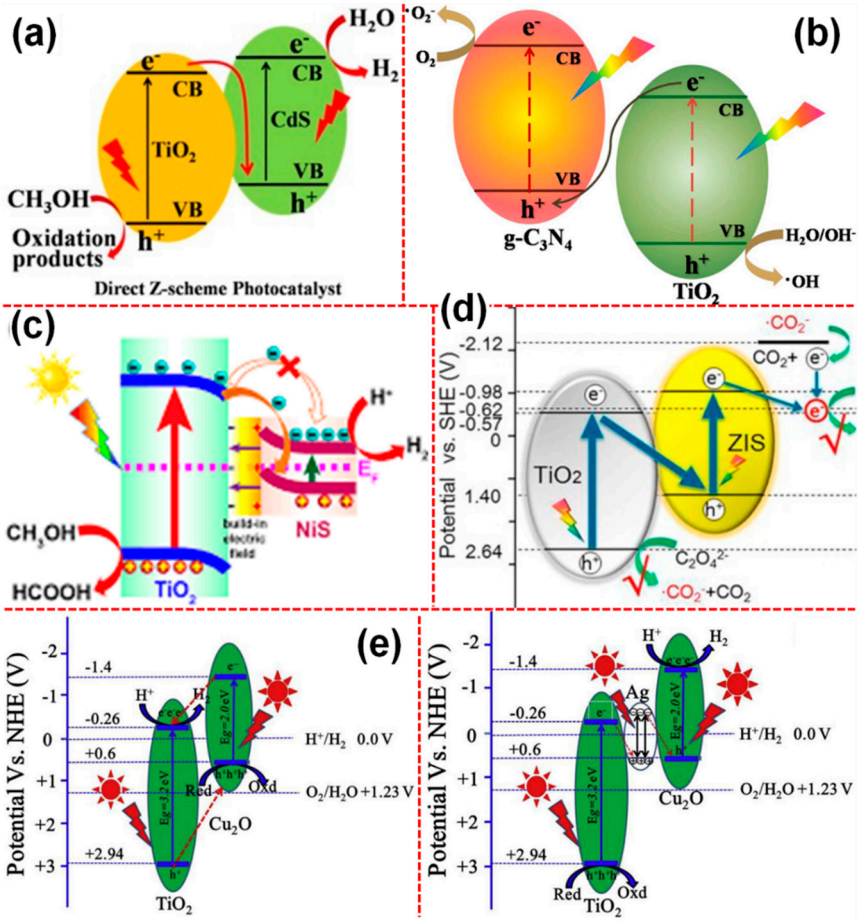

Figure 8. Charge transfer mechanism in various Z-scheme-based TiO_2 photocatalysts, (**a**) CdS/TiO_2, (**b**) $g\text{-}C_3N_4/TiO_2$, (**c**) NiS/TiO_2, (**d**) $ZnIn_2S_4/TiO_2$, and (**e**) TiO_2–Ag–Cu_2O (reproduced with permission from refs. [121,124,126–128], respectively).

3.5. Plasmonic TiO_2

Plasmonic photocatalysis is one of the emerging and interesting concepts in this field [130]. These types of photocatalysts make use of the plasmonic nanoparticles to harvest energy in the visible region [131]. It extends the absorption range of the photocatalyst in UV-visible-IR region [132]. The plasmonic nanoparticles also play an important role in alerting the charge transfer mechanism in the host photocatalysts. The plasmon-mediated process in photocatalysts can occur in four different ways, (i) direct migration of carriers from the plasmonic particles to photocatalyst, (ii) indirect migration of carriers between the plasmonic particles and photocatalyst via the localized surface plasmon resonance (LSPR), (iii) localized plasmonic heating, and (iv) radiative transfer of photons from the plasmonic particles to the photocatalyst, where these photons will excite the photocatalyst to generate the electron hole pairs in the system [131–133]. However, the origins and functions of plasmonic photocatalysts are under hot debate.

Noble metals such as Ag, Au, Pd, and Pt have been integrated with TiO_2 to produce the TiO_2-based plasmonic photocatalysts. Among them, Ag–TiO_2 has been relatively largely studied with different configurations [134–137]. Plasmonic sensitization conventionally happens by the deposition of plasmonic nanoparticles (NPs) onto the surface of the host photocatalyst. However, there have been other configurations such as core-shell structuring [137], filling up the plasmonic NPs into the pores of the host photocatalyst, and composite-like formation [135]. As aforementioned, the plasmonic nanoparticles can extend the light absorption in the visible region and they can also substantially influence the charge transfer kinetics the photocatalyst. However, there are essentially two pathways

proposed regarding their charge transfer, which is either from the (i) plasmonic NPs to photocatalyst or (ii) photocatalyst to plasmonic NPs [130]. As a result, it has also been proposed that the scheme of such charge transfer is also determined by the relative band edge potential, conducting type (n/p-type), and work function of the photocatalyst and plasmonic metal, respectively, and also determined by the light source that is used to excite the plasmonic photocatalyst system, as shown in Figure 9a–b [134,138].

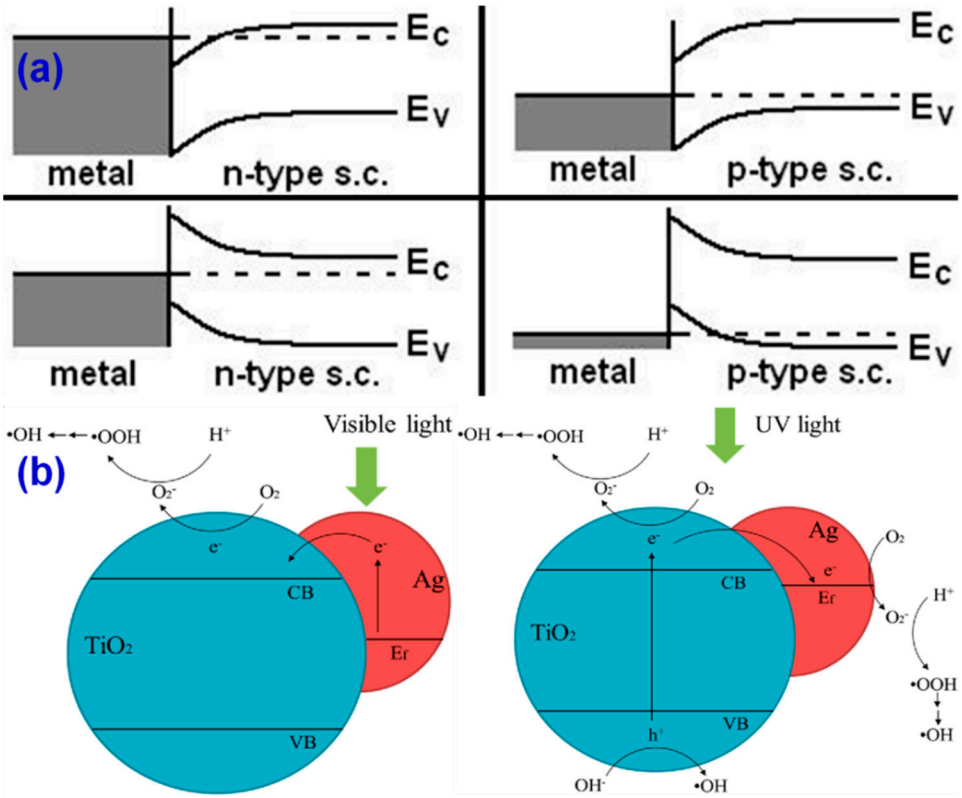

Figure 9. (**a**) Band bending occurs in the metal-semiconductor junction and (**b**) charge transfers in plasmonic photocatalyst, depending upon the light source irradiated (reproduced with permission from refs. [134,138], respectively).

As depicted in Figure 9a [138], the work function of the metal nanoparticle with respect to the host semiconductor also directs the course of charge transfer in the plasmonic photocatalyst. For instance, the work function of Au, Ag, and anatase TiO_2 has the work function of 5.23, 4.25–4.37, and 5.10 eV, respectively, where the Au–TiO_2 and Ag–TiO_2 follow the Schottky-junction and Ohmic-junction, respectively, for the charge transfer in the system, as shown in Figure 10a,b [139]. Compared to the Ag and Au, the surface plasmon resonance (SPR) properties of Pt/Pd-deposited TiO_2 has been less explored [140]. However, these metal NPs have been explored as a co-catalyst for various photocatalyst systems [141–143]. This is because the plasmonic peak of Pt NPs appears below 450 nm, while the SPR properties of Ag and Au can be well tuned in visible to IR region, and therefore, the Pt and Pd NPs have not been typically used for developing the plasmonic photocatalysts [144–146].

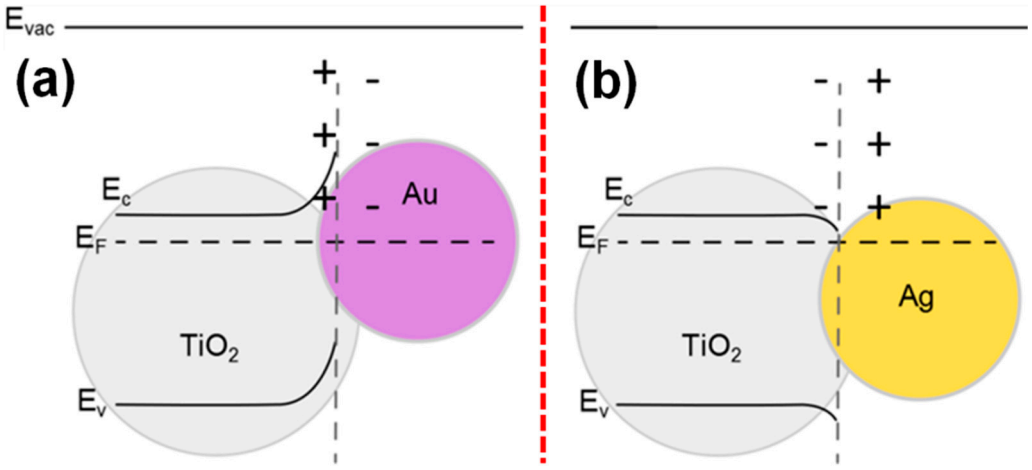

Figure 10. Work function dependent band-bending in (**a**) Au/TiO_2, (**b**) Ag/TiO_2 plasmonic systems (reproduced with permission from ref. [139]).

3.6. Ferroelectrics Modified TiO_2

Ferroelectrics are defined by the spontaneous electric polarization that can be induced by an external electric field, where the induced spontaneous polarization will be permanent in the material and it essentially originates from the off-center displacements of ions in a non-centrosymmetric crystal system [147]. In ferroelectric materials, the internal screening induced by the free carriers and the bulk defects lead to the distribution of charge carriers in the near surface of the material, which essentially creates a space-charge region and band bending in the system [148]. These features greatly help in the photocatalytic process. The bands of ferroelectrics bend at the near the surface or interface region, depending upon the positive or negative spontaneous polarizations, as shown in Figure 11a,b [149].

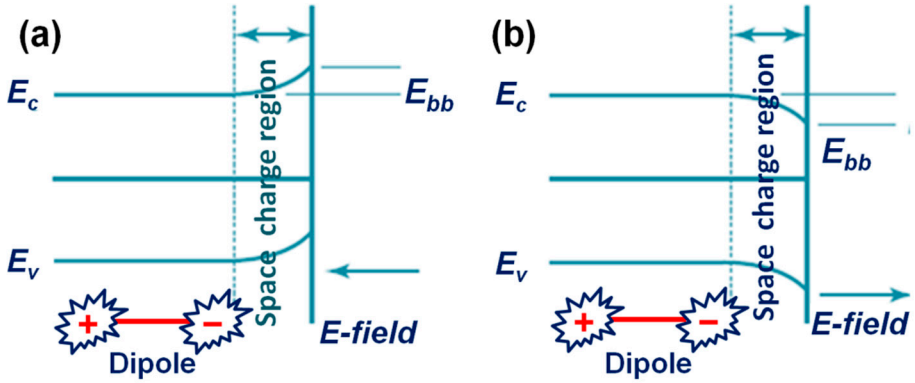

Figure 11. Schematic diagram of band bending in a ferroelectric material; (**a**) a surface with negative polarity and (**b**) a surface with positive polarity.

For instance, in a negatively polarized surface, the electrons will be depleted from the surface, which leads to a creation of a spatial-charge layer (depletion layer) with "upward" band-bending. On the other hand, in a positively polarized surface, the electrons will be accumulated for screening, which leads to a "downward" band bending in the system along with formation of a spatial accumulation charge layer. Thereby, these interesting features in ferroelectric, along with such deformed migration of charge carriers, largely helpful to exhibit exotic photo-active chemical properties [150,151]. The features such as the spontaneous polarization, deformed migration of carriers, surface charges, band bending process, and the external and/or internal screening effects altogether direct the photo-induced charge carriers in a ferroelectric toward an effective oxidation and reduction reaction for various photocatalytic applications [152–158].

Ferroelectric materials such as $BaTiO_3$ [159–161], $BiFeO_3$ [162,163], $PbTiO_3$ [164] have been successfully integrated with TiO_2 to produce ferroelectric-TiO_2 photocatalysts. Zhang et al. have explained how the ferroelectric phenomenon influences the photocatalytic activity of the system, where they demonstrated it using $BiFeO_3/TiO_2$ system [162]. They proposed a plausible energy level for the $BiFeO_3/TiO_2$ system, as shown in Figure 12a,b. According to this diagram, the energy levels at the interface of $BiFeO_3$ (BFO) and TiO_2 are strongly influenced by the induced polarization in $BiFeO_3$, where it bends the band of BFO upward when the polarization in negative (i.e., away from the surface) and downward when the polarization is positive (i.e., towards the surface). Under such circumstances, the photo-induced electrons in negative domains are impeded by the energy barrier at the interface; meanwhile, in positive domains, the electrons are moved to the interface, in such a way that it facilitates the photocatalytic activity with enough redox abilities of the excited charge carriers in the system [163].

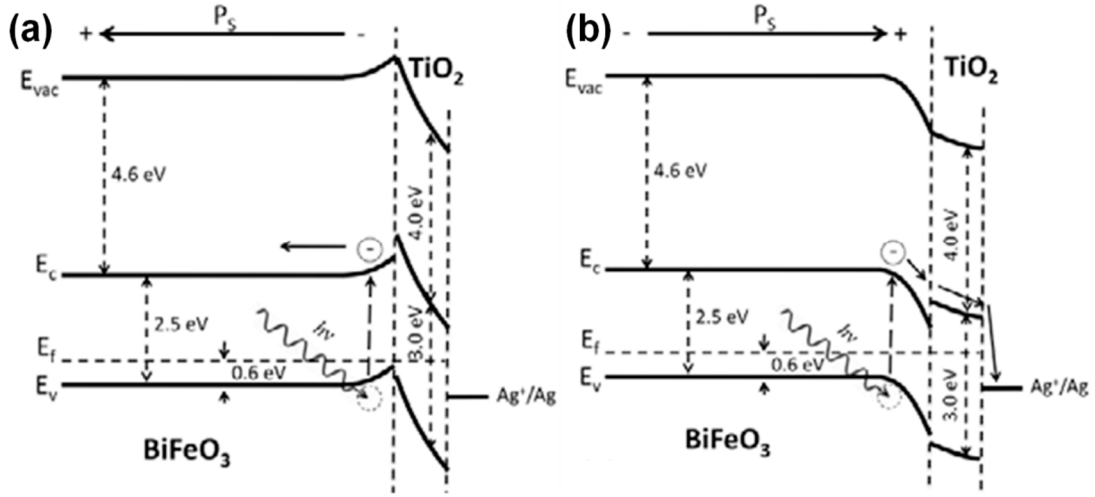

Figure 12. The energy bands at the $BiFeO_3/TiO_2$ interface bend (**a**) upward and (**b**) downward corresponding to the applied polarization (reproduced with permission from ref. [162]).

3.7. Carbon-Based TiO_2 Composites

Carbon-based materials-modified TiO_2 photocatalysts demonstrate significant enhancements in the photocatalytic process due to various reasons such as (i) high surface area, (ii) enhanced electrical conductivity, (iii) tunable optical properties, (iv) improved surface adsorption efficiency, and (v) controllable structural features [165–167]. These properties essentially help improve the overall properties of the photocatalysts. For instance, the enhanced surface area populates more catalytic-sites on the surface of the catalysts. The enhanced electrical conductivity improves the charge separation and transportation characteristics of the system. The tunable optical properties help activate the photocatalyst under a desirable light source such as visible light and/or sunlight. The improved surface adsorption essentially paves the way for the adsorption of surrounding molecules onto the surface of the photocatalyst that eventually enhances the interfacial interaction of the photocatalyst and molecules. Finally, the controllable structural features of carbon materials such as quantum dots (fullerenes) [168–170], 2D materials (graphene, g-C_3N_4) [171,172], 1D materials (carbon nanotubes (CNTs), carbon fibers) [173–176], and 3D materials (carbon spheres, flowers) [177,178] offer unique charge transportations and improve the overall efficiency of the carbon-based photocatalytic materials.

TiO_2 has been modified by the variety of carbon-based materials such as carbon doping, carbon coating, composites with activated carbon, graphene/graphene oxide/reduced-graphene oxide, g-C_3N_4, CNTs, carbon fibers, anisotropic carbon structures, etc. [165–178]. The general photocatalytic mechanisms of these carbon-based TiO_2 systems are summarized in Figure 13a–d [168,179–181] Yu et al. [168], have reported the mechanism of carbon quantum dots (CQDs)-integrated TiO_2 towards photocatalytic H_2 production. The CQDs play a dual vital role in the improved photocatalytic properties.

During the photocatalytic excitation under UV light, the CQDs act as (i) electron reservoirs and (ii) photo-sensitizers. The former role of CQDs essentially plays a role in trapping the photo-generated electrons from the conduction band of TiO_2 and facilitates the enhanced process of electrons-holes separation. On the other hand, the latter characteristics of π-conjugated CQDs is to sensitize the TiO_2 as similar to the organic dyes, towards making it a visible light active "dyade"-like structure, where it gives the electrons to the CB of TiO_2 and leads to the visible light-driven hydrogen production (Figure 13a) [168].

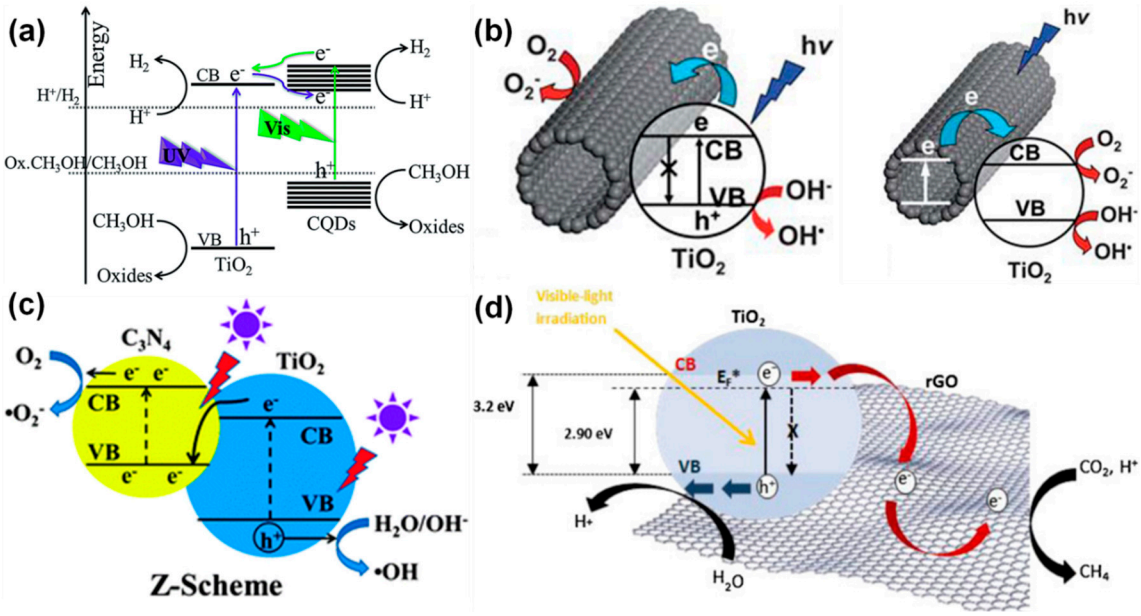

Figure 13. Photocatalytic mechanism in various carbon-TiO_2 systems, (**a**) carbon QD-TiO_2, (**b**) carbon nanotubes (CNT)-TiO_2, (**c**) g-C_3N_4-rGo-TiO_2, (**d**) rGO-TiO_2 (reproduced with permission from refs. [168,179–181], respectively).

The carbon nanotubes (CNTs), owing to their large electron-storage capacity (per electron for every 32 C-atoms), accept the photo-induced electrons from the supported semiconductor and, thereby, they largely hinder the recombination of charge carriers [179]. It is believed that the excellent conductive nature of the CNTs promotes the electron-hole separation via the formation of a heterojunction between CNTs and semiconductors. For instance, as similar to the carbon QDs, the CNTs also play a dual role in the photocatalytic process. Accordingly, the freely moving electrons in the excited TiO_2 get transferred into the CNTs scaffolds, where the excess holes in the VB in TiO_2 are set to reach and react with the H_2O and OH^- to generate radicals such $OH^\bullet$ as shown in Figure 13b [179]. On the other hand, it is known that TiO_2 is UV-driven, but it is observed that the CNTs-TiO_2 nanocomposites have become visible light driven, which is attributed to the photo-sensitizing effect of CNTs. In this scenario, the photo-induced electrons in CNTs (sensitizers) get injected into the CB of TiO_2 and lead to reducing the adsorbed molecular oxygen to form the superoxide species. In parallel, the holes in these positively charged CNTs react with H_2O and form $OH^\bullet$ radicals, as shown in Figure 13b.

Yu et al. [180] have demonstrated that the coupling between TiO_2 and g-C_3N_4 cannot lead to the formation of heterojunction; rather, it always tends to form the Z-scheme-based photocatalyst system. Based on their experiments, they have explained the phenomenon that if TiO_2 and g-C_3N_4 form a heterojunction, then the following scenario will emerge. Under the UV exposure, the photo-induced holes will get transferred from the VB of TiO_2 to that of the g-C_3N_4 and the electrons will get transferred from CB of g-C_3N_4 to that of the TiO_2. As a result, the holes of g-C_3N_4 cannot oxidize the adsorbed H_2O or OH^- to form the $OH^\bullet$ radicals due to the higher potential of VB of g-C_3N_4 with respect to the H_2O/OH^- couple. Such a process eventually leads to the lower oxidation, thereby the photocatalytic

efficiency of the system is much lower than the TiO_2. However, the observed photocatalytic efficiency of TiO_2/g-C_3N_4 is higher than the individual counterparts, which essentially means that this system forms a direct Z-scheme system without the electron mediator, as shown in Figure 13c [180].

The photocatalytic mechanism in the reduced graphene oxide (rGO)-TiO_2 composite has been proposed by Tan et al. [181] as shown in Figure 13d. In the rGO-TiO_2 composite, the d and π orbital of TiO_2 and rGO, respectively, matches well in their energy levels and they overlap each other well (d-π). As a result, rGO is bound to serve as an electron-collector as well as a transporter towards effectively separating the photo-induced electron-hole pairs, which eventually enhances the lifetime of the charge carriers as well, and thereby the photocatalytic efficiency of the rGO-TiO_2 system [182–185].

3.8. 2D-Transition Metal Chalcogenides Modified TiO_2

It is well established that the large surface-to-volume ratio of 2D nanostructures can provide more surface-active sites for the photocatalytic reactions. The planar structure of 2D materials essentially favors the charge transportations across the interfaces of the catalyst and surrounding phases and thereby it drastically improves the photocatalytic efficiencies [186]. Moreover, as compared to other nanostructures, the 2D nanostructures exhibit exotic properties owing to the atomic arrangements with surface atomic elongation and structural-disorder characteristics [187]. These interesting physical structure-induced properties of 2D materials largely contribute in enhancing the photo-stability and chemical durability of the photocatalyst. Furthermore, 2D materials, due to their flat band potential and effective band bending at the interface, help tune the band gap energies and band-edge positions of the photocatalysts [188]. Specifically, when these 2D materials couple with the other metal and metal oxides, their unique 2D structures serve as a matrix for those integrated materials and enhance the optical and electrical properties of the system as a whole [189–191]. In this direction, the 2D transition metal chalcogenides (2D TMC) with general chemical formula of MX_2, M = Mo, or W and X = S, Se, or Te serve as both the independent or composite photocatalytic materials [191]. Accordingly, TiO_2 has been modified with these 2D TMC materials to avail their structural features and unique properties towards various photocatalytic applications.

Among the listed 2D TMC materials, the MoS_2/TiO_2 system has been largely explored for the photocatalytic applications [192–197]. Interestingly, the charge transfer in this system depends upon the photon energy used to excite the system. The Figure 14a,b shows the charge transfer in a MoS_2/TiO_2 system that irradiated under UV and visible light, respectively [198,199]. When the MoS_2/TiO_2 system irradiated under UV light, the electrons that were excited in TiO_2 will be transferred to the attached MoS_2 nanosheets; thereby, this process significantly limits the electron hole recombination and promotes carrier separation by effectively transporting to the adsorbed H^+ ions to reduce them to produce molecular hydrogen. On the other hand, when the MoS_2/TiO_2 system is irradiated under visible light, the electron transfer occurs from the MoS_2 to TiO_2, as shown in Figure 14b [199]. It should be noted that the TiO_2 used in this study is doped with N species that facilitates visible light absorption in TiO_2 as well. Therefore, the coupling of MoS_2 with TiO_2 promotes the excited electrons to the CB of TiO_2 from the CB of MoS_2. The further photocatalytic reactions essentially occur via the conventional redox reactions on the surface of the photocatalyst.

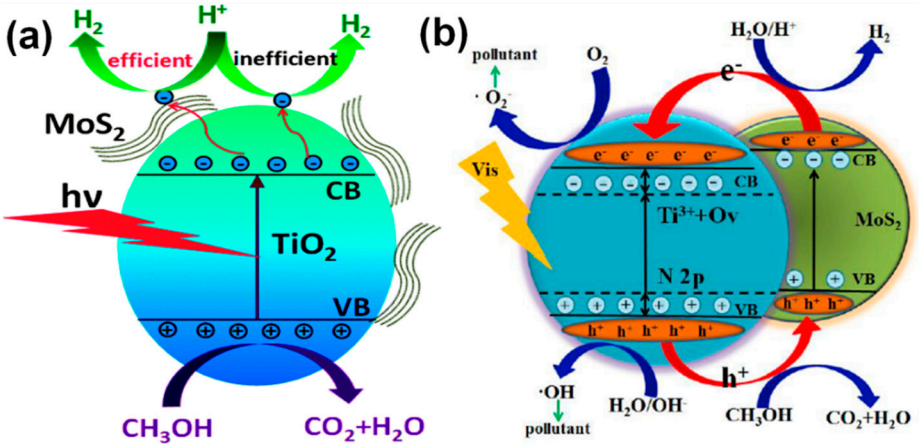

Figure 14. Photocatalytic charge transfer process in MoS_2/TiO_2 under the irradiation of (**a**) UV light and (**b**) visible light (reproduced with permission from refs. [198,199]).

Zhang et al., have reported the possible charge transfer mechanism in P25-TiO_2/MoS_2 and P25-TiO_2/WS_2 systems under UV-visible irradiation [200]. Accordingly, the excited electrons in P25-TiO_2/MoS_2 migrate from the CB of TiO_2 to the CB of MoS_2, while it occurs vice versa in the P25-TiO_2/WS_2 system, as shown in Figure 15a,b [200]. The observed charge transfer mechanism is essentially due to the relative band-edge potentials of the semiconductors involved in the composite.

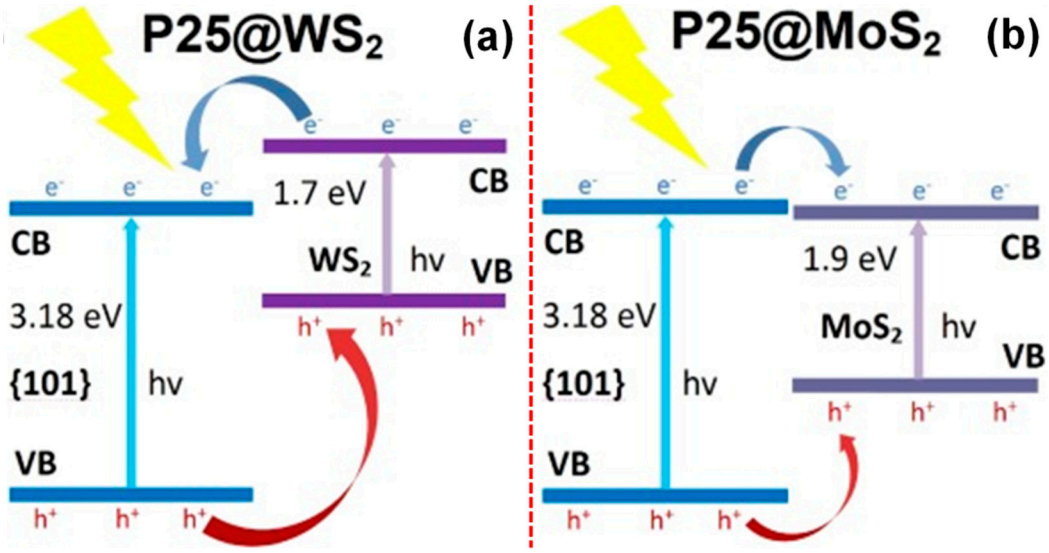

Figure 15. Photocatalytic charge transfer mechanism in (**a**) P25-TiO_2/WS_2 and (**b**) P25-TiO_2/MoS_2 (reproduced with permission from ref. [200]).

Similar to the aforementioned systems, there are alternative hypotheses to explain the charge transfer mechanism in $MoSe_2/TiO_2$ system. Chu et al. [201] and Shen et al. [202] have proposed that the $MoSe_2/TiO_2$ follows the heterojunction mechanism towards the charge transfer process in the system, as shown in Figure 16a [201]. Accordingly, the type-II heterostructure, which formed between $MoSe_2$ and TiO_2, facilitates the electron transfer from the CB of $MoSe_2$ to that of TiO_2 and reduces the recombination process, prolongs the lifetime of the carriers, and provides an enhanced conductivity in the system towards transporting the carriers to the surrounding for the effective photocatalytic process. On the other hand, Zheng et al. proposed that this system follows the Z-scheme to transfer the charges from the TiO_2 to $MoSe_2$ [203]. According to their hypothesis, the $MoSe_2/TiO_2$ (nanotubes) photocatalyst could not form a type-II heterojunction. This may be because of the reason that the

holes in TiO_2 VB are likely to migrate into the $MoSe_2$ VB if type-II has been formed. However, their experimental investigations using ESR and PL demonstrated that the proposed charge is not possible, owing to the low potential of 0.98 V that cannot effectively oxidize the adsorbed surface H_2O to produce $OH^{\bullet}$ radicals. Therefore, the photo-generated electrons in the CB of TiO_2 might have been transferred and recombined with the holes in $MoSe_2$ VB, leaving the holes in the VB of TiO_2 and electrons in the CB of $MoSe_2$ via constructing a 'direct Z-Scheme' to augment the photocatalytic redox reactions in the system, as shown in Figure 16b [203]. Similarly, the WS_2/TiO_2 system has also been explored for various photocatalytic applications and their mechanisms [204–210].

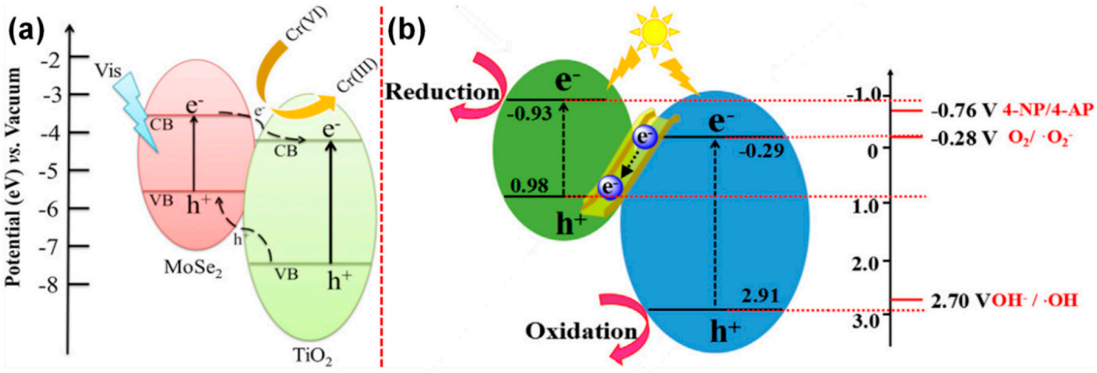

Figure 16. Charge transfer mechanism in $MoSe_2/TiO_2$ (**a**) heterojunction and (**b**) Z-scheme (reproduced with permission from refs. [201,203]).

3.9. Metal-Organic Framework-TiO_2 Composites

Metal–organic frameworks (MOFs) are an exotic class of crystalline materials with inherent porous structures. MOFs are constructed using the metal clusters that interconnected by organic ligands built into a 3D networked structure. Their unique properties, such as the well-ordered porosity, very high specific surface area, and tunable surface chemistry, have made them a promising material for various applications, including photocatalysis. MOFs can be reliable photocatalytic materials due to semiconductor-like properties. In addition, they possess high surface area that largely facilitates enhanced surface catalytic activities; the metal clusters play a role in the effective absorption of incident photons and charge separation, while the ligands favor the charge transportations in the system. However, the major issue in MOFs is the moderate charge separation that considerably reduces the overall photocatalytic efficiency of the MOFs [211–216].

Yao et al. proposed the observed superior photocatalytic efficiency of TiO_2@-NH_2-UiO-66 composites towards the degradation of styrene [217]. According to their findings, (i) the plenty of available interconnected nanopore facilitated the enhanced and rapid diffusion of the surrounding styrene molecules into the pores of MOFs, where the encapsulated TiO_2 effectively oxidized the molecules with the produced oxidation radical species, and (ii) the linkers in MOFs acted as antenna to augment the light absorption and sensitize the TiO_2 and led to the effective absorption of light towards the transportation of charge carriers in the system; thereby, it demonstrated excellent photocatalytic activity [217].

Similarly, the photocatalytic efficiency of TiO_2/NH_2-UiO-66 nanocomposites towards CO_2 reduction has been demonstrated by Crake et al. [218]. Based on their observations, the composite of NH_2-UiO-66 and TiO_2 can lead to the formation of type-II heterojunction. This could essentially be because of the factor that the CB position of NH_2-UiO-66 lies at −0.6 eV, while the TiO_2 CB lies at a more negative potential at −0.28 eV, as shown in Figure 17a [218]. They have further proposed that the photocatalytic activity of TiO_2/NH_2-UiO-66 nanocomposites was mainly ruled out by (i) the concentration of TiO_2, (ii) the effective charge separation characteristics of NH_2-UiO-66, and (iii) the enhanced availability of charge carriers at the interface of the TiO_2/NH_2-UiO-66 system. Ling et al. have synthesized a ternary nanocomposite composed of TiO_2/UiO-66-NH_2/graphene oxide and studied

towards the photocatalytic dye (RhB) degradation and H_2 evolution [219]. They have reported that, under the visible excitation, the electrons tend to transfer from RhB* to CB of MOFs to CB of TiO_2 due to the cascading potential of these systems. Under such circumstances, the integrated GO captures the electrons from the CB of TiO_2 that eventually enhances charge separation, thereby accelerating the dye removal. On the other hand, the electrons from GO further migrate to the Pt and lead to the H_2 production. It is also possible that the electrons from RhB* can get directly injected into Pt and produce H_2, as shown in Figure 17b [219]. Similarly, there have been other TiO_2/MOFs-based photocatalytic systems reported [220–225].

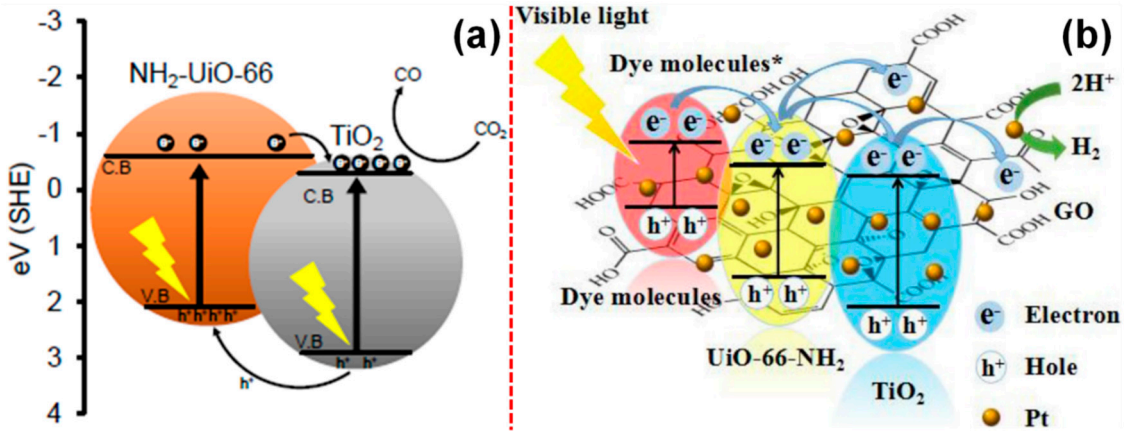

Figure 17. Photocatalytic charge transfer process in (**a**) TiO_2/NH_2-UiO-66 for CO_2 reduction and (**b**) TiO_2/NH_2-UiO-66/GO/Pt for dye removal and H_2 production (reproduced with permission from refs. [218,219]).

3.10. Reduced/Defective/Colored TiO_{2-x} Photocatalysts

The off-stoichiometricity in TiO_2, which is induced by processes such as self-doping by Ti^{3+} ions and oxygen vacancy creations (V_o), plays an important role in enhancing the visible light absorption and photocatalytic efficiency of the TiO_2 materials [226–230]. Based on such a modification approach, TiO_2 has been synthesized in a variety of "colors" such as black, blue, red, and yellow. The reduced band gap energy in off-stoichiometric TiO_2 essentially originates due to the formation of localized energy states (0.75–1.18eV) underneath the CB minimum of the TiO_2 [231]. As compared to any other modification strategies, the self-doping and/or oxygen vacancy creation is more favorable for maintaining the intrinsic properties of the TiO_2 as well as to introduce the visible light absorption characteristics and enhance the photocatalytic efficiencies of TiO_2 [232–234].

The first black-TiO_2 was produced by Chen et al. with band gap energy of around 1.0 eV via high-pressure hydrogenation process in the crystalline TiO_2 [235]. The general mechanism for the formation of black TiO_2 is broadly attributed to the presence of Ti^{3+} by self-doping, formation of hydroxyl groups on the surface, oxygen vacancies, Ti-H bonds, and the formation of H-energy states in the mid-gap of the TiO_2 band structure, which eventually dispersed the VB in TiO_2, as shown in Figure 18a [235]. Zhu et al. synthesized the stable blue TiO_2 nanoparticles [236] and proposed the origin that the observed blue color could be due to the high concentration of Ti^{3+} defects in the bulk and the formation of mid-gap electronic energy states beneath the band gap of TiO_2. As a result, the observed enhanced photocatalytic properties were attributed to their unique structural features, which is the disordered-core/ordered-shell-like structure. This essentially means that the TiO_2 was stoichiometric at the surface while it was off-stoichiometric in the core. These features collectively improved the overall photocatalytic efficiencies of the blue TiO_2 by enhancing the charge separation and transportation, as shown in Figure 18b [236].

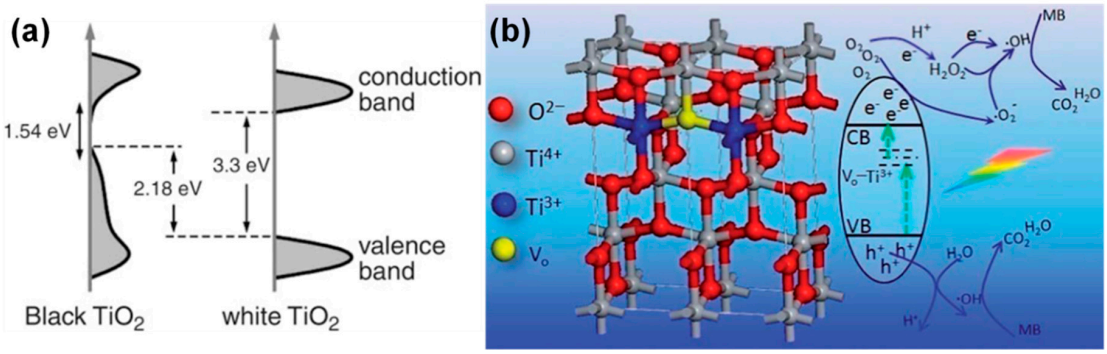

Figure 18. Band gap structure of (**a**) black-TiO_2 and (**b**) blue-TiO_2 (reproduced with permission from refs. [235,236]).

Wu et al. developed ultra-small yellow TiO_2 nanoparticles via simple sol-gel process with UV treatment technique. Based on their experimental findings, the origin of the observed yellow color of TiO_2 could be due to titanium vacancies (V_{Ti}) and titanium interstitials (Ti_i) as shown in Figure 19a [237]. Interestingly, Liu et al. prepared the red anatase TiO_2 via a gradient co-doping of B-N into the system. It was observed that the band gap energy varied from 1.94 eV on the surface to 3.22 eV in the core, as shown in Figure 19b [238].

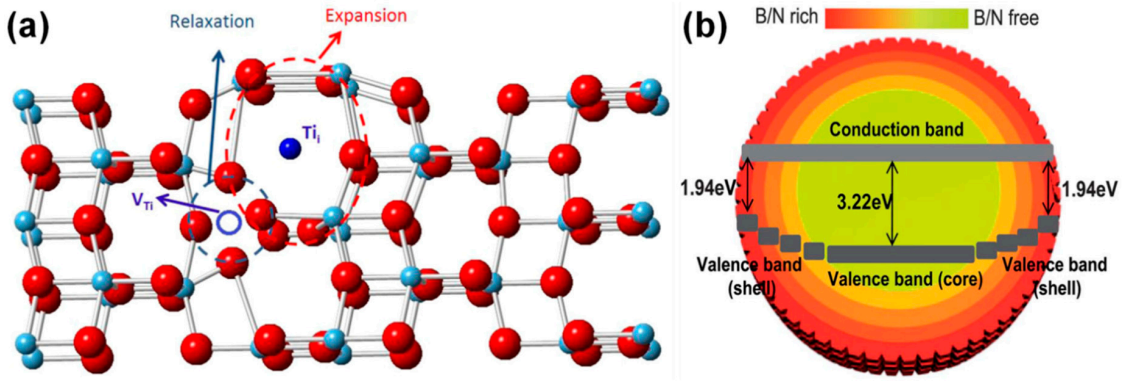

Figure 19. (**a**) Structure of yellow-TiO_2 and (**b**) anatase red TiO_2 via gradient B-N co-doping (reproduced with permission from refs. [237,238]).

Ren et al. reported that the $NaBH_4$ reduced TiO_2 photocatalysts with a range of colors such as white, light-yellow, light-grey, and dark-grey, which were prepared by varying the concentration of the reducing agent $NaBH_4$, as shown in Figure 20a [239]. The observed color variation was attributed to the self-doping of Ti^{3+} ions into the TiO_2. Similarly, Fan et al. reported the synthesis of TiO_2 with white, dark brown, light brown, yellow, light yellow, gray, yellowish gray, and yellowish white color (Figure 20b) that were derived from the amorphous hydrated TiO_2 through hydroxylated and N-doping process with a controlled degree of disorders using a heating treatment technique [240]. In this study, the observed color variation was attributed to the heating process that turned the Ti–OH bonds in amorphous TiO_2 into the Ti–O bonds that transformed the disordered TiO_6 octahedron into a regular 3D structure. As a result, the formed hydroxylated anatase TiO_2 with enhanced degree of disorder strongly influenced the optical transition in TiO_2 and narrowed down the band gap energy. Further, these colored TiO_2 materials have also demonstrated enhanced photocatalytic efficiencies towards the degradation of acid fuchsin under visible light.

Figure 20. Photographic images of the (**a**) chemically reduced TiO_2 with increasing concentration of $NaBH_4$ and (**b**) hydroxylated and N-doped anatase TiO_2 that were derived from the amorphous hydrate TiO_2 at the increasing processing temperature (reproduced with permission from refs. [239,240]).

4. Summary and Outlook

Undoubtedly, TiO_2 is indeed an interesting material for various photocatalytic applications. As described, the fundamental photocatalytic process involves the excitation of photo-induced carriers and their successful transfer to the surface to produce the desired redox species towards the designated photocatalytic application. The versatile applications emerge essentially due to the produced redox species with appropriate energy, which is dictated by the band edge potential of the photocatalyst. Since TiO_2 inherently meets such requirements, it has been successfully used for various photocatalytic applications. However, TiO_2 has limitations such as its wide-band gap, moderate charge separation efficiency, etc. To overcome such limitations, TiO_2 has been both physically and chemically modified. Accordingly, herein we provided a glimpse on the various modifications that were performed on TiO_2 towards enhancing its photocatalytic efficiencies. These modifications include morphological modifications, anionic-cationic doping, heterojunction formations, Z-scheme formations, plasmonic integrations, ferroelectric integrations, carbon-based materials integrations, 2D transition metal chalcogenide integrations, metal–organic framework integrations, and defects inducements in TiO_2. We also have discussed the charge transfer mechanism that manifests in these various modified-TiO_2 photocatalytic systems.

TiO_2 can be a prototype photocatalyst, which can be used to design new photocatalytic materials. The meticulous investigations on TiO_2 for their photocatalytic mechanism can be better applied towards its effective applications in photocatalysis. In this direction, the further improvement in TiO_2 could be the establishment of techniques to intrinsically modify the TiO_2 towards their photocatalytic enhancements. Such known techniques are the inducement of defective structures in TiO_2 through self-doping, atoms in interstitial positions, oxygen-, and Ti-vacancies. For instance, instead of doping the N atoms into TiO_2, the O atoms can be partially replaced by N atoms to form oxy-nitrides and so the oxy-phosphates, oxy-sulfur, oxy-carbon, etc., can be formed by partially replacing the O atoms with P, S, and C, respectively. These modifications may lead to the formation of entirely different TiO_2-based materials with possibly new crystal phase and structure and can exhibit enhanced photocatalytic efficiencies. Towards applications, TiO_2 can be explored for new photocatalytic processes such as the production of H_2/O_2 from the atmospheric vapor, dark-photocatalysis, hydrogen storage, biodiesel productions, etc. TiO_2 should be consistently explored towards further understanding of their photocatalytic mechanisms and finding new photocatalytic applications.

Funding: This work was supported by the Natural Science and Engineering Research Council of Canada (NSERC) through the Collaborative Research and Development (CRD), Strategic Project (SP), and Discovery Grants (DG). MS gratefully acknowledges the Department of Science and Technology, Govt. of India for the funding support through the DST-INSPIRE Faculty Award [DST/INSPIRE/04/2016/002227, 14-02-2017].

Acknowledgments: We would also like to thank EXP Inc. and SiliCycle Inc. for their support.

Conflicts of Interest: The authors declare no conflict of interest. The funders had no role in the design of the study; in the collection, analyses, or interpretation of data; in the writing of the manuscript, or in the decision to publish the results.

References

1. Fujishima, A.; Honda, K. Electrochemical photolysis of water at a semiconductor electrode. *Nature* **1972**, *238*, 37–38. [CrossRef]
2. Schrauzer, G.N.; Guth, T.D. Photocatalytic reactions. 1. Photolysis of water and photoreduction of nitrogen on titanium dioxide. *J. Am. Chem. Soc.* **1977**, *99*, 7189–7193. [CrossRef]
3. Kiwi, J.; Gratzel, M. Projection, size factors, and reaction dynamics of colloidal redox catalysts mediating light induced hydrogen evolution from water. *J. Am. Chem. Soc.* **1979**, *101*, 7214–7217. [CrossRef]
4. Kawai, T.; Sakata, T. Conversion of carbohydrate into hydrogen fuel by a photocatalytic process. *Nature* **1980**, *286*, 474–476. [CrossRef]
5. Sato, S.; White, J.M. Photoassisted water-gas shift reaction over platinized titanium dioxide catalysts. *J. Am. Chem. Soc.* **1980**, *102*, 7206–7210. [CrossRef]
6. Bagheri, S.; Yousefi, A.T.; Do, T.O. Photocatalytic pathway toward degradation of environmental pharmaceutical pollutants: Structure, kinetics and mechanism approach. *Catal. Sci. Technol.* **2017**, *7*, 4548–4569. [CrossRef]
7. Moser, J.; Gratzel, M. Light-induced electron transfer in colloidal semiconductor dispersions: Single vs. dielectronic reduction of acceptors by conduction-band electrons. *J. Am. Chem. Soc.* **1983**, *105*, 6547–6555. [CrossRef]
8. Bahnemann, D.; Henglein, A.; Lilie, J.; Spanhel, L. Flash photolysis observation of the absorption spectra of trapped positive holes and electrons in colloidal titanium dioxide. *J. Phys. Chem.* **1984**, *88*, 709–711. [CrossRef]
9. Nozik, A.J.; Williams, F.; Nenadovic, M.T.; Rajh, T.; Micic, O.I. Size quantization in small semiconductor particles. *J. Phys. Chem.* **1985**, *89*, 397–399.
10. Anpo, M.; Shima, T.; Kodama, S.; Kubokawa, Y. Photocatalytic hydrogenation of propyne with water on small-particle titania: Size quantization effects and reaction intermediates. *J. Phys. Chem.* **1987**, *91*, 4305–4310. [CrossRef]
11. Hong, A.P.; Bahnemann, D.W.; Hoffmann, M.R. Cobalt (II) tetrasulfophthalocyanine on titanium dioxide. 2. Kinetics and mechanisms of the photocatalytic oxidation of aqueous sulfur dioxide. *J. Phys. Chem.* **1987**, *91*, 6245–6251. [CrossRef]
12. Zhang, J.L.; Minagawa, M.; Matsuoka, M.; Yamashita, H.; Anpo, M. Photocatalytic decomposition of NO on Ti-HMS mesoporous zeolite catalysts. *Catal. Lett.* **2000**, *66*, 241–243. [CrossRef]
13. Frank, S.N.; Bard, A.J. Heterogeneous photocatalytic oxidation of cyanide ion in aqueous solutions at titanium dioxide powder. *J. Am. Chem. Soc.* **1977**, *99*, 303–304. [CrossRef]
14. Halmann, M. Photoelectrochemical reduction of aqueous carbon dioxide on p-type gallium phosphide in liquid junction solar cells. *Nature* **1978**, *275*, 115–116. [CrossRef]
15. Anpo, M.; Chiba, K.; Tomonari, M.; Coluccia, S.; Che, M.; Fox, M.A. Photocatalysis on Native and Platinum-Loaded TiO_2 and ZnO Catalysts-Origin of Different Reactivities on Wet and Dry Metal Oxides. *Bull. Chem. Soc. Jpn.* **1991**, *64*, 543–551. [CrossRef]
16. Domen, K.; Naito, S.; Soma, M.; Onishi, T.; Tamaru, K. Photocatalytic decomposition of water vapour on an NiO-$SrTiO_3$ catalyst. *J. Chem. Soc. Chem. Commun.* **1980**, *12*, 543–544. [CrossRef]
17. Boonstra, A.H.; Mutsaers, C. Relation between the photoadsorption of oxygen and the number of hydroxyl groups on a titanium dioxide surface. *J. Phys. Chem.* **1975**, *79*, 1694–1698. [CrossRef]
18. Yun, C.; Anpo, M.; Kubokawa, Y. UV irradiation-induced fission of a C=C or C≡C bond adsorbed on TiO_2. *J. Chem. Soc. Chem. Commun.* **1980**, 609. [CrossRef]
19. Anpo, M.; Nakaya, H.; Kodama, S.; Kubokawa, Y.; Domen, K.; Onishi, T. Photocatalysis over binary metal oxides. Enhancement of the photocatalytic activity of titanium dioxide in titanium-silicon oxides. *J. Phys. Chem.* **1986**, *90*, 1633–1636. [CrossRef]

20. Anpo, M.; Kawamura, T.; Kodama, S.; Maruya, K.; Onishi, T. Photocatalysis on titanium-aluminum binary metal oxides: Enhancement of the photocatalytic activity of titania species. *J. Phys. Chem.* **1988**, *92*, 438–440. [CrossRef]
21. Dohshi, S.; Takeuchi, M.; Anpo, M. Photoinduced superhydrophilic properties of Ti-B binary oxide thin films and their photocatalytic reactivity for the decomposition of NO. *J. Nanosci. Nanotechnol.* **2001**, *1*, 337–342. [CrossRef] [PubMed]
22. Liu, Y.; Li, Z.; Green, M.; Just, M.; Li, Y.Y.; Chen, X. Titanium dioxide nanomaterials for photocatalysis. *J. Phys. D: Appl. Phys.* **2017**, *50*, 193003. [CrossRef]
23. Jenny, S.; Matsuoka, M.; Takeuchi, M.; Zhang, J.; Horiuchi, Y.; Anpo, M.; Detlef, W. Bahnemann. Understanding TiO_2 photocatalysis: Mechanisms and materials. *Chem. Rev.* **2014**, *114*, 9919–9986.
24. Hashimoto, K.; Irie, H.; Fujishima, A. TiO_2 photocatalysis: A historical overview and future prospects. *Jpn. J. Appl. Phys.* **2005**, *44*, 8269. [CrossRef]
25. Coronado, D.R.; Gattorno, G.R.; Pesqueira, M.E.E.; Cab, C.; de Coss, R.; Oskam, G. Phase-pure TiO_2 nanoparticles: Anatase, brookite and rutile. *Nanotechnology* **2008**, *19*, 145605. [CrossRef] [PubMed]
26. Zhang, J.; Zhou, P.; Liu, J.; Yu, J. New understanding of the difference of photocatalytic activity among anatase, rutile and brookite TiO_2. *Phys. Chem. Chem. Phys.* **2014**, *16*, 20382–20386.
27. Linsebigler, A.L.; Lu, G.; Yates, J.T., Jr. Photocatalysis on TiO_2 surfaces: Principles, mechanisms, and selected results. *Chem. Rev.* **1995**, *95*, 735–758. [CrossRef]
28. Girish Kumar, S.; Gomathi Devi, L. Review on modified TiO_2 photocatalysis under UV/visible light: Selected results and related mechanisms on interfacial charge carrier transfer dynamics. *J. Phys. Chem. A.* **2011**, *115*, 13211–13241. [CrossRef]
29. de Lasa, H.; Serrano, B.; Salaices, M. Establishing Photocatalytic Kinetic Rate Equations: Basic Principles and Parameters. In *Photocatalytic Reaction Engineering*; Springer: Boston, MA, USA, 2005.
30. Ravelli, D.; Dondi, D.; Fagnonia, M.; Albini, A. Photocatalysis. A multi-faceted concept for green chemistry. *Chem. Soc. Rev.* **2009**, *38*, 1999–2011. [CrossRef]
31. Nakata, K.; Fujishima, A. TiO_2 photocatalysis: Design and applications. *J. Photochem. Photobio. C Photochem. Rev.* **2012**, *13*, 169–189. [CrossRef]
32. Parrino, F.; De Pasquale, C.; Palmisano, L. Influence of surface-related phenomena on mechanism, selectivity, and conversion of TiO_2-induced photocatalytic reactions. *ChemSusChem* **2019**, *12*, 589–602. [CrossRef] [PubMed]
33. Fujishima, A.; Zhang, X.; Tryk, D.A. TiO_2 photocatalysis and related surface phenomena. *Surf. Sci. Rep.* **2008**, *63*, 515–582. [CrossRef]
34. Pan, X.; Yang, M.Q.; Fu, X.; Zhang, N.; Xu, Y.-J. Defective TiO_2 with oxygen vacancies: Synthesis, properties and photocatalytic applications. *Nanoscale* **2013**, *5*, 3601–3614. [CrossRef] [PubMed]
35. Scanlon, D.O.; Dunnill, C.W.; Buckeridge, J.; Shevlin, S.A.; Logsdail, A.J.; Woodley, S.M.; Catlow, C.R.; Powell, M.J.; Palgrave, R.G.; Parkin, I.P.; et al. Band alignment of rutile and anatase TiO_2. *Nat. Mater.* **2013**, *12*, 798–801. [CrossRef] [PubMed]
36. Guo, Q.; Zhou, C.; Ma, Z.; Ren, Z.; Fan, H.; Yang, X. Fundamental Processes in Surface Photocatalysis on TiO_2. In *Heterogeneous Photocatalysis*; Green Chemistry and Sustainable Technology; Colmenares, J., Xu, Y.J., Eds.; Springer: Berlin/Heidelberg, Germany, 2016.
37. Yalavarthi, R.; Naldoni, A.; Kment, S.; Mascaretti, L.; Kmentová, H.; Tomanec, O.; Schmuki, P.; Zboril, R. Radiative and non-radiative recombination pathways in mixed-phase TiO_2 nanotubes for PEC water-splitting. *Catalysts* **2019**, *9*, 204. [CrossRef]
38. Nguyen, C.C.; Vu, N.N.; Do, T.O. Efficient hollow double-shell photocatalysts for the degradation of organic pollutants under visible light and in darkness. *J. Mater. Chem. A* **2016**, *4*, 4413–4419. [CrossRef]
39. Sakar, M.; Nguyen, C.C.; Vu, M.H.; Do, T.O. Materials and mechanisms of photo-assisted chemical reactions under light and dark: Can day-night photocatalysis be achieved? *ChemSusChem* **2018**, *11*, 809–820. [CrossRef]
40. Dinh, C.T.; Pham, M.H.; Seo, Y.; Kleitz, F.; Do, T.O. Design of multicomponent photocatalysts for hydrogen production under visible light using water-soluble titanate nanodisks. *Nanoscale* **2014**, *6*, 4819–4829. [CrossRef]
41. Dinh, C.T.; Seo, Y.; Nguyen, T.D.; Kleitz, F.; Do, T.O. Controlled synthesis of titanate nanodisks as versatile building blocks for the design of hybrid nanostructures. *Angew. Chem. Int. Ed.* **2012**, *51*, 6608–6612. [CrossRef]

42. Dinh, C.T.; Nguyen, T.D.; Kleitz, F.; Do, T.O. Shape-controlled synthesis of highly crystalline titania nanocrystals. *ACS Nano* **2009**, *11*, 3737–3743. [CrossRef]
43. Ng, J.; Pan, J.H.; Sun, D.D. Hierarchical assembly of anatase nanowhiskers and evaluation of their photocatalytic efficiency in comparison to various one-dimensional TiO_2 nanostructures. *J. Mater. Chem.* **2011**, *21*, 11844–11853. [CrossRef]
44. Conceição, D.S.; Ferreira, D.P.; Graça, C.A.L.; Julio, M.F.; Ilharco, L.M.; Velosa, A.C.; Santos, P.F.; Vieira Ferreira, L.F. Photochemical and photocatalytic evaluation of 1D titanate/TiO_2 based nanomaterials. *Appl. Surf. Sci.* **2017**, *392*, 418–429. [CrossRef]
45. Gordon, T.R.; Cargnello, M.; Paik, T.; Mangolini, F.; Weber, R.T.; Fornasiero, P.; Murray, C.B. Nonaqueous synthesis of TiO_2 nanocrystals using TiF_4 to engineer morphology, oxygen vacancy concentration, and photocatalytic activity. *J. Am. Chem. Soc.* **2012**, *134*, 6751–6761. [CrossRef] [PubMed]
46. Ziarati, A.; Badiei, A.; Luque, R. Black Hollow TiO_2 nanocubes: Advanced nanoarchitectures for efficient visible light photocatalytic applications. *Appl. Catal. B Environ.* **2018**, *238*, 177–183. [CrossRef]
47. Dinh, C.T.; Nguyen, T.D.; Kleitz, F.; Do, T.O. A novel single-step route based on solvothermal technique to shape-controlled titanium dioxide nanocrystals. *Can. J. Chem. Eng.* **2012**, *90*, 8–17. [CrossRef]
48. Kang, X.; Song, X.Z.; Han, Y.; Cao, J.; Tan, Z. Defect-engineered TiO_2 hollow spiny nanocubes for phenol degradation under visible light irradiation. *Sci. Rep.* **2018**, *8*, 5904. [CrossRef] [PubMed]
49. Zhou, X.; Liu, N.; Schmuki, P. Photocatalysis with TiO_2 nanotubes: "Colorful" reactivity and designing site-specific photocatalytic centers into TiO_2 nanotubes. *ACS Catal.* **2017**, *7*, 3210–3235. [CrossRef]
50. Zhao, Q.E.; Wen, W.; Xia, Y.; Wu, J.M. Photocatalytic activity of TiO_2 nanorods, nanowires and nanoflowers filled with TiO_2 nanoparticles. *Thin Solid Films* **2018**, *648*, 103–107. [CrossRef]
51. Nguyen, C.C.; Vu, N.N.; Do, T.O. Recent advances in the development of sunlight-driven hollow structure photocatalysts and their applications. *J. Mater. Chem. A* **2015**, *7*, 8187–8208. [CrossRef]
52. Li, M.; Chen, Y.; Li, W.; Li, X.; Tian, H.; Wei, X.; Ren, Z.; Han, G. Ultrathin anatase TiO_2 nanosheets for high-performance photocatalytic hydrogen production. *Small* **2017**, *13*, 1604115. [CrossRef]
53. Choi, S.K.; Kim, S.; Lim, S.K.; Park, H. Photocatalytic comparison of TiO_2 Nanoparticles and Electrospun TiO_2 nanofibers: Effects of mesoporosity and interparticle charge transfer. *J. Phys. Chem. C* **2010**, *114*, 16475–16480. [CrossRef]
54. Ribeiro, R.A.P.; de Lazaro, S.R.; de Oliveira, C.R. Band-Gap engineering for photocatalytic applications: Anionic and cationic doping of TiO_2 anatase. *Curr. Phys. Chem.* **2016**, *6*, 22–27. [CrossRef]
55. Yalçın, Y.; Kılıç, M.; Çınar, Z. The role of non-metal doping in TiO_2 photocatalysis. *J. Adv. Oxid. Technol.* **2016**, *13*, 281–296. [CrossRef]
56. Chen, X.; Burda, C. The electronic origin of the visible-light absorption properties of C-, N- and S-doped TiO_2 nanomaterials. *J. Am. Chem. Soc.* **2008**, *130*, 5018–5019. [CrossRef] [PubMed]
57. Emy, M.S.; Sharifah, B.A.H. Effect of band gap engineering in anionic-doped TiO_2 photocatalyst. *Appl. Surf. Sci.* **2017**, *391*, 326–336.
58. Wang, H.; Lewis, J.P. Second-generation photocatalytic materials: Anion-doped TiO_2. *J. Phys. Condens. Matter* **2006**, *18*, 421–434. [CrossRef]
59. Kuznetsov, V.N.; Serpone, N. on the origin of the spectral bands in the visible absorption spectra of visible-light-active TiO_2 specimens analysis and assignments. *J. Phys. Chem. C* **2009**, *113*, 15110–15123. [CrossRef]
60. Serpone, N. Is the band gap of pristine TiO_2 narrowed by anion- and cation-doping of titanium dioxide in second-generation photocatalysts? *J. Phys. Chem. B* **2006**, *110*, 24287–24293. [CrossRef]
61. Fan, W.Q.; Bai, H.Y.; Zhang, G.H.; Yan, Y.S.; Liu, C.B.; Shi, W.D. Titanium dioxide macroporous materials doped with iron: Synthesis and photo-catalytic properties. *CrystEngComm* **2014**, *16*, 116–122. [CrossRef]
62. Chang, S.M.; Liu, W.S. The roles of surface-doped metal ions (V, Mn, Fe, Cu, Ce, and W) in the interfacial behavior of TiO_2 photocatalysts. *Appl. Catal. B Environ.* **2014**, *156*, 466–475. [CrossRef]
63. Hahn, R.; Stark, M.; Killian, M.S.; Schmuki, P. Photocatalytic properties of in situ doped TiO_2-nanotubes grown by rapid breakdown anodization. *Catal. Sci. Technol.* **2013**, *3*, 1765–1770. [CrossRef]
64. Ishii, M.; Towlson, B.; Harako, S.; Zhao, X.W.; Komuro, S.; Hamilton, B. Roles of electrons and holes in the luminescence of rare-earth-doped semiconductors. *Electr. Commun. Jpn.* **2013**, *96*, 1–7. [CrossRef]

65. Tobaldi, D.M.; Pullar, R.C.; Gualtieri, A.F.; Seabra, M.P.; Labrincha, J.A. Sol-gel synthesis, characterisation and photocatalytic activity of pure, W-, Ag- and W/Ag codoped TiO_2 nanopowders. *Chem. Eng. J.* **2013**, *214*, 364–375. [CrossRef]
66. de Lima, J.F.; Harunsani, M.H.; Martin, D.J.; Kong, D.; Dunne, P.W.; Gianolio, D.; Kashtiban, R.J.; Sloan, J.; Serra, O.A.; Tang, J.; et al. Control of chemical state of cerium in doped anatase TiO_2 by solvothermal synthesis and its application in photocatalytic water reduction. *J. Mater. Chem. A* **2015**, *3*, 9890–9898. [CrossRef]
67. Li, H.; Liu, J.; Qian, J.; Li, Q.; Yang, J. Preparation of Bi-doped TiO_2 nanoparticles and their visible light photocatalytic performance. *Chin. J. Catal.* **2014**, *35*, 1578–1589. [CrossRef]
68. Klaysri, R.; Wichaidit, S.; Tubchareon, T.; Nokjan, S.; Piticharoenphun, S.; Mekasuwandumrong, O.; Praserthdam, P. Impact of calcination atmospheres on the physiochemical and photocatalytic properties of nanocrystalline TiO_2 and Si-doped TiO_2. *Ceram. Int.* **2015**, *41*, 11409–11417. [CrossRef]
69. Zhao, Y.; Liu, J.; Shi, L.; Yuan, S.; Fang, J.; Wang, Z.; Zhang, M. Solvothermal preparation of Sn^{4+} doped anatase TiO_2 nanocrystals from peroxo-metal-complex and their photocatalytic activity. *Appl. Catal. B Environ.* **2011**, *103*, 436–443. [CrossRef]
70. Carneiro, J.O.; Azevedo, S.; Fernandes, F.; Freitas, E.; Pereira, M.; Tavares, C.J.; Lanceros-Mendez, S.; Teixeira, V. Synthesis of iron-doped TiO_2 nanoparticles by ball-milling process: The influence of process parameters on the structural, optical, magnetic, and photocatalytic properties. *J. Mater. Sci.* **2014**, *49*, 7476–7488. [CrossRef]
71. Makdee, A.; Unwiset, P.; Chanapattharapol, K.C.; Kidkhunthod, P. Effects of Ce addition on the properties and photocatalytic activity of TiO_2, investigated by X-ray absorption spectroscopy. *Mater. Chem. Phys.* **2018**, *213*, 431–443. [CrossRef]
72. Unwiset, P.; Makdee, A.; Chanapattharapol, K.C.; Kidkhunthod, P. Effect of Cu addition on TiO_2 surface properties and photocatalytic performance: X-ray absorption spectroscopy analysis. *J. Phys. Chem. Solids* **2018**, *120*, 231–240. [CrossRef]
73. Zhang, D.R.; Liu, H.L.; Han, S.Y.; Piao, W.X. Synthesis of Sc and V-doped TiO_2 nanoparticles and photodegradation of rhodamine-B. *J. Indus. Eng. Chem.* **2013**, *19*, 1838–1844. [CrossRef]
74. Ould-Chikh, S.; Proux, O.; Afanasiev, P.; Khrouz, L.; Hedhili, M.N.; Anjum, D.H.; Harb, M.; Geantet, C.; Basset, J.; Puzenat, E. Photocatalysis with chromium-doped TiO_2: Bulk and surface doping. *ChemSusChem* **2014**, *7*, 1361–1371. [CrossRef] [PubMed]
75. Deng, Q.R.; Xia, X.H.; Guo, M.L.; Gao, Y.; Shao, G. Mn-doped TiO_2 nanopowders with remarkable visible light photocatalytic activity. *Mater. Lett.* **2011**, *65*, 2051–2054. [CrossRef]
76. Sun, L.; Zhai, J.; Li, H.; Zhao, Y.; Yang, H.; Yu, H. Study of homologous elements: Fe, Co, and Ni dopant effects on the photoreactivity of TiO_2 nanosheets. *ChemCatChem* **2014**, *6*, 339–347. [CrossRef]
77. Karunakaran, C.; Abiramasundari, G.; Gomathisankar, P.; Manikandan, G.; Anandi, V. Cu-doped TiO_2 nanoparticles for photocatalytic disinfection of bacteria under visible light. *J. Colloid Interface Sci.* **2010**, *352*, 68–74. [CrossRef] [PubMed]
78. Aware, D.V.; Jadhav, S.S. Synthesis, characterization and photocatalytic applications of Zn-doped TiO_2 nanoparticles by sol–gel method. *Appl. Nanosci.* **2016**, *6*, 965–972. [CrossRef]
79. Jiang, X.; Gao, Y.; Li, C.; You, F.; Yao, J.; Ji, Y. Preparation of hollow yttrium-doped TiO_2 microspheres with enhanced visible-light photocatalytic activity. *Mater. Res. Express* **2019**, *6*, 065510. [CrossRef]
80. Gao, B.; Lim, T.M.; Subagio, D.P.; Lim, T.T. Zr-doped TiO_2 for enhanced photocatalytic degradation of bisphenol A. *Appl. Catal. A Gen.* **2010**, *375*, 107–115. [CrossRef]
81. Kou, Y.; Yang, J.; Li, B.; Fu, S. Solar photocatalytic activities of porous Nb-doped TiO_2 microspheres by coupling with tungsten oxide. *Mater. Res. Bull.* **2015**, *63*, 105–111. [CrossRef]
82. Avilés-García, O.; Espino-Valencia, J.; Romero, R.; Rico-Cerda, J.L.; Arroyo-Albiter, M.; Natividad, R. W and Mo doped TiO_2: Synthesis, characterization and photocatalytic activity. *Fuel* **2017**, *198*, 31–41. [CrossRef]
83. Hao, H.Y.; He, C.X.; Tian, B.Z.; Zhang, J.L. Study of photocatalytic activity of Cd-doped mesoporous nanocrystalline TiO_2 prepared at low temperature. *Res. Chem. Intermed.* **2009**, *35*, 705. [CrossRef]
84. Chandan, H.R.; Sakar, M.; Ashesh, M.; Ravishankar, T.N.; Ramakrishnappa, T.; Sergio, R.T.; Geetha Balakrishna, R. Observation of oxo-bridged yttrium in TiO_2 nanostructures and their enhanced photocatalytic hydrogen generation under UV/Visible light irradiations. *Mater. Res. Bull.* **2018**, *104*, 212–219.

85. Štengl, V.; Bakardjieva, S.; Murafa, N. Preparation and photocatalytic activity of rare earth doped TiO_2 nanoparticles. *Mater. Chem. Phys.* **2009**, *114*, 217–226. [CrossRef]
86. Al-Maliki, F.J.; Al-Lamey, N.H. Synthesis of Tb-doped titanium dioxide nanostructures by sol–gel method for environmental photocatalysis applications. *J. Sol-Gel Sci. Technol.* **2017**, *81*, 276–283. [CrossRef]
87. Singh, K.; Harish, S.; Kristya, A.P.; Shivani, V.; Archana, J.; Navaneethan, M.; Shimomura, M.; Hayakawa, Y. Erbium doped TiO_2 interconnected mesoporous spheres as an efficient visible light catalyst for photocatalytic applications. *Appl. Surf. Sci.* **2018**, *449*, 755–763. [CrossRef]
88. Jiang, X.; Li, C.; Liu, S.; Zhang, F.; You, F.; Yao, C. The synthesis and characterization of ytterbium-doped TiO_2 hollow spheres with enhanced visible-light photocatalytic activity. *RSC Adv.* **2017**, *7*, 24598–24606. [CrossRef]
89. Shwetharani, R.; Sakar, M.; Chandan, H.R.; Geetha Balakrishna, R. Observation of simultaneous photocatalytic degradation and hydrogen evolution on the lanthanum modified TiO_2 nanostructures. *Mater. Lett.* **2018**, *218*, 262–265. [CrossRef]
90. Ravishankar, T.N.; Nagaraju, G.; Dupont, J. Photocatalytic activity of Li-doped TiO_2 nanoparticles: Synthesis via ionic liquid-assisted hydrothermal route. *Mater. Res. Bull.* **2016**, *78*, 103–111. [CrossRef]
91. Shivaraju, H.P.; Midhun, G.; Anil Kumar, K.M.; Pallavi, S.; Pallavi, N.; Behzad, S. Degradation of selected industrial dyes using Mg-doped TiO_2 polyscales under natural sun light as an alternative driving energy. *Appl. Water Sci.* **2017**, *7*, 3937–3948. [CrossRef]
92. Fu, W.; Ding, S.; Wang, Y.; Wu, L.; Zhang, D.; Pan, Z.; Wang, R.; Zhang, Z.; Qiu, S. F, Ca co-doped TiO_2 nanocrystals with enhanced photocatalytic activity. *Dalton Trans.* **2014**, *43*, 16160–16163. [CrossRef] [PubMed]
93. Xie, W.; Li, R.; Xu, Q. Enhanced photocatalytic activity of Se-doped TiO_2 under visible light irradiation. *Sci. Rep.* **2018**, *8*, 8752. [CrossRef] [PubMed]
94. Nguyen, C.C.; Dinh, C.T.; Do, T.O. Hollow Rh/Sr-codoped TiO_2 photocatalyst for efficient sunlight-driven organic compound degradation. *RSC Adv.* **2017**, *7*, 3480–3487. [CrossRef]
95. Murashkina, A.A.; Murzin, P.D.; Rudakova, A.V.; Ryabchuk, V.K.; Emeline, A.V.; Detlef, W. Bahnemann. Influence of the dopant concentration on the photocatalytic activity: Al-doped TiO_2. *J. Phys. Chem. C* **2015**, *119*, 24695–24703. [CrossRef]
96. Liqiang, J.; Honggang, F.; Baiqi, W.; Dejun, W.; Baifu, X.; Shudan, L.; Jiazhong, S. Effects of Sn dopant on the photoinduced charge property and photocatalytic activity of TiO_2 nanoparticles. *Appl. Catal. B Environ.* **2006**, *62*, 282–291. [CrossRef]
97. Nan, W.; Xing, L.; Yanling, Y.; Tingting, G.; Xiaoxuan, Z.; Siyang, J.; Tingting, Z.; Yi, S.; Zhiwei, Z. Enhanced photocatalytic degradation of sulfamethazine by Bi-doped TiO_2 nano-composites supported by powdered activated carbon under visible light irradiation. *Sep. Purif. Technol.* **2019**, *211*, 673–683.
98. Li, W. Influence of electronic structures of doped TiO_2 on their photocatalysis. *Phys. Status Solidi R* **2015**, *9*, 10–27. [CrossRef]
99. Boulbar, E.L.; Millon, E.; Leborgne, C.B.; Cachoncinlle, C.; Hakim, B.; Ntsoenzok, E. Optical properties of rare earth-doped TiO_2 anatase and rutile thin films grown by pulsed-laser deposition. *Thin Solid Films* **2014**, *553*, 13–16. [CrossRef]
100. Shwetharani, R.; Sakar, M.; Fernando, C.A.N.; Binas, V.; Geetha Balakrishna, R. Recent advances and strategies applied to tailor energy levels, active sites and electron mobility in titania and its doped/composite analogues for hydrogen evolution in sunlight. *Catal. Sci. Technol.* **2019**, *9*, 12–46. [CrossRef]
101. Ma, Y.T.; Li, S.D. Photocatalytic activity of TiO_2 nanofibers with doped La prepared by electrospinning method. *J. Chin. Chem. Soc.* **2015**, *62*, 380–384. [CrossRef]
102. Borlaf, M.; Colomer, M.T.; de Andrés, A.; Cabello, F.; Serna, R.; Moreno, R. TiO_2/Eu^{3+} thin films with high photoluminescence emission prepared by electrophoretic deposition from nanoparticulate sols. *Eur. J. Inorg. Chem.* **2014**, *30*, 5152–5159. [CrossRef]
103. Du, J.; Li, B.; Huang, J.; Zhang, W.; Peng, H.; Zou, J. Hydrophilic and photocatalytic performances of lanthanum doped titanium dioxide thin films. *J. Rare Earth* **2013**, *31*, 992–996. [CrossRef]
104. Maddila, S.; Oseghe, E.O.; Jonnalagadda, S.B. Photocatalyzed ozonation by Ce doped TiO_2 catalyst degradation of pesticide Dicamba in water. *J. Chem. Technol. Biotechnol.* **2016**, *91*, 385–393. [CrossRef]
105. Choudhury, B.; Borah, B.; Choudhury, A. Extending photocatalytic activity of TiO_2 nanoparticles to visible region of illumination by doping of cerium. *Photochem. Photobiol.* **2012**, *88*, 257–264. [CrossRef] [PubMed]

106. Vu, T.T.D.; Mighri, F.; Ajji, A.; Do, T.O. Synthesis of titanium dioxide/cadmium sulfide nanosphere particles for photocatalyst applications. *Ind. Eng. Chem. Res.* **2014**, *53*, 3888–3897. [CrossRef]
107. Wang, H.; Zhang, L.; Chen, Z.; Hu, J.; Li, S.; Wang, Z.; Liu, J.; Wang, X. Semiconductor heterojunction photocatalysts: Design, construction, and photocatalytic performances. *Chem. Soc. Rev.* **2014**, *43*, 5234–5244. [CrossRef] [PubMed]
108. Afroz, K.; Moniruddin, M.; Bakranov, N.; Kudaibergenov, S.; Nuraje, N. A heterojunction strategy to improve the visible light sensitive water splitting performance of photocatalytic materials. *J. Mater. Chem. A* **2018**, *6*, 21696–21718. [CrossRef]
109. Bessekhouad, Y.; Robert, D.; Weber, J.V. Photocatalytic activity of Cu_2O/TiO_2, Bi_2O_3/TiO_2 and $ZnMn_2O_4/TiO_2$ heterojunctions. *Catal. Today* **2005**, *101*, 315–321. [CrossRef]
110. Liu, J.; Yang, S.; Wu, W.; Tian, Q.; Cui, S.; Dai, Z.; Ren, F.; Xiao, X.; Jiang, C. 3D Flowerlike α-Fe_2O_3@TiO_2 core-shell nanostructures: General synthesis and enhanced photocatalytic performance. *ACS Sustain. Chem. Eng.* **2015**, *3*, 2975–2984. [CrossRef]
111. Xia, Y.; Yin, L. Core-shell structured α-Fe_2O_3@TiO_2 nanocomposites with improved photocatalytic activity in visible light region. *Phys. Chem. Chem. Phys.* **2013**, *15*, 18627–18634. [CrossRef]
112. Lin, Z.; Liu, P.; Yan, J.; Yang, G. Matching energy levels between TiO_2 and α-Fe_2O_3 in a core-shell nanoparticle for the visible-light photocatalysis. *J. Mater. Chem. A* **2015**, *3*, 14853–14863. [CrossRef]
113. Moniz, S.J.A.; Shevlin, S.A.; Martin, D.J.; Guo, Z.X.; Tang, J. Visible-light driven heterojunction photocatalysts for water splitting—A critical review. *Energy Environ. Sci.* **2015**, *8*, 731–759. [CrossRef]
114. Ge, J.; Zhang, Y.; Heo, Y.J.; Park, S.J. Advanced design and synthesis of composite photocatalysts for the remediation of wastewater: A review. *Catalysts* **2019**, *9*, 122. [CrossRef]
115. 115. Danlian, H.; Sha, C.; Zeng, G.; Gong, X.; Zhou, C.; Cheng, M.; Xue, W.; Yan, X.; Li, J. Artificial Z-scheme photocatalytic system: What have been done and where to go? *Coordination Chem. Rev.* **2019**, *385*, 44–80.
116. Bard, A.J. Photoelectrochemistry and heterogeneous photo-catalysis at semiconductors. *J. Photochem.* **1979**, *10*, 59–75. [CrossRef]
117. Jiang, W.; Zong, X.; An, L.; Hua, S.; Miao, X.; Luan, S.; Wen, Y.; Tao, F.F.; Sun, Z. Consciously constructing heterojunction or direct z-scheme photocatalysts by regulating electron flow direction. *ACS Catal.* **2018**, *8*, 2209–2217. [CrossRef]
118. Xu, Q.; Zhang, L.; Yu, J.; Wageh, S.; Al-Ghamdi, A.A.; Jaroniec, M. Direct Z-scheme photocatalysts: Principles, synthesis, and applications. *Mater. Today* **2018**, *21*, 1042–1063. [CrossRef]
119. Qi, K.; Cheng, B.; Yu, J.; Ho, W. A review on TiO_2-based Z-scheme photocatalysts. *Chin. J. Catal.* **2017**, *38*, 1936–1955. [CrossRef]
120. Li, H.; Tu, W.; Zhou, Y.; Zou, Z. Z-scheme photocatalytic systems for promoting photocatalytic performance: Recent progress and future challenges. *Adv. Sci.* **2016**, *3*, 1500389. [CrossRef]
121. Meng, A.; Zhu, B.; Zhong, B.; Zhang, L.; Cheng, B. Direct Z-scheme TiO_2/CdS hierarchical photocatalyst for enhanced photocatalytic H_2-production activity. *Appl. Surface Sci.* **2017**, *422*, 518–527. [CrossRef]
122. Dinh, C.T.; Pham, M.H.; Kleitz, F.; Do, T.O. Design of water-soluble CdS-titanate-nickel nanocomposites for photocatalytic hydrogen production under sunlight. *J. Mater. Chem. A* **2013**, *1*, 13308–13313. [CrossRef]
123. Jo, W.K.; Natarajan, T.S. Influence of TiO_2 morphology on the photocatalytic efficiency of direct Z-scheme g-C_3N_4/TiO_2 photocatalysts for isoniazid degradation. *Appl. Surf. Sci.* **2017**, *422*, 518–527.
124. Zhou, D.; Chen, Z.; Yang, Q.; Dong, X.; Zhang, J.; Qin, L. In-situ construction of all-solid-state Z-scheme g-C_3N_4/TiO_2 nanotube arrays photocatalyst with enhanced visible-light-induced properties. *Solar Energy Mater. Solar Cells* **2016**, *157*, 399–405. [CrossRef]
125. Liao, W.; Murugananthan, M.; Zhang, Y. Synthesis of Z-scheme g-C_3N_4-Ti^{3+}/TiO_2 material: An efficient visible light photoelectrocatalyst for degradation of phenol. *Phys. Chem. Chem. Phys.* **2015**, *17*, 8877–8884. [CrossRef] [PubMed]
126. Xu, F.; Zhang, L.; Cheng, B.; Yu, J. Direct Z-scheme TiO_2/NiS core-shell hybrid nanofibers with enhanced photocatalytic H_2-production activity. *ACS Sustain. Chem. Eng.* **2018**, *6*, 12291–12298. [CrossRef]
127. Li, Q.; Xia, Y.; Yang, C.; Lv, K.; Lei, M.; Li, M. Building a direct Z-scheme heterojunction photocatalyst by $ZnIn_2S_4$ nanosheets and TiO_2 hollowspheres for highly-efficient artificial photosynthesis. *Chem. Eng. J.* **2018**, *349*, 287–296. [CrossRef]
128. Fu, J.; Cao, S.; Yu, J. Dual Z-scheme charge transfer in TiO_2-Ag-Cu_2O composite for enhanced photocatalytic hydrogen generation. *J. Materiomics* **2015**, *1*, 124–133. [CrossRef]

129. Pan, L.; Zhang, J.; Jia, X.; Ma, Y.H.; Zhang, X.; Wang, L.; Zou, J.J. Highly efficient Z-scheme WO_{3-x} quantum dots/TiO_2 for photocatalytic hydrogen generation. *Chin. J. Catal.* **2017**, *38*, 253–259. [CrossRef]
130. Zhang, X.; Chen, Y.L.; Liu, R.S.; Tsai, D.P. Plasmonic photocatalysis. *Rep. Prog. Phys.* **2013**, *76*, 046401. [CrossRef] [PubMed]
131. Wang, P.; Huang, B.; Dai, Y.; Whangbo, M.H. Plasmonic photocatalysts: Harvesting visible light with noble metal nanoparticles. *Phys. Chem. Chem. Phys.* **2012**, *14*, 9813–9825. [CrossRef]
132. Wu, J.; Zhang, Z.; Liu, B.; Fang, Y.; Wang, L.; Dong, B. UV-Vis-NIR-driven plasmonic photocatalysts with dual-resonance modes for synergistically enhancing H_2 generation. *Sol. RRL* **2018**, *2*, 1800039. [CrossRef]
133. Dinh, C.T.; Hoang, Y.; Kleitz, F.; Do, T.O. Three-dimensional ordered assembly of thin-shell Au/TiO_2 hollow nanospheres for enhanced visible-light-driven photocatalysis. *Angew. Chem. Int. Ed.* **2014**, *53*, 6618–6623. [CrossRef] [PubMed]
134. He, Y.; Basnet, P.; Hunyadi Murph, S.E.; Zhao, Y. Ag nanoparticle embedded TiO_2 composite nanorod arrays fabricated by oblique angle deposition: Toward plasmonic photocatalysis. *ACS Appl. Mater. Interfaces* **2013**, *5*, 11818–11827. [CrossRef] [PubMed]
135. Chen, Z.; Fang, L.; Dong, W.; Zheng, F.; Shena, M.; Wang, J. Inverse opal structured Ag/TiO_2 plasmonic photocatalyst prepared by pulsed current deposition and its enhanced visible light photocatalytic activity. *J. Mater. Chem. A* **2014**, *2*, 824–832. [CrossRef]
136. Dinh, C.T.; Nguyen, T.D.; Kleitz, F.; Do, T.O. A new route to size and population control of silver clusters on colloidal TiO_2 nanocrystals. *ACS Appl. Mater. Interfaces* **2011**, *3*, 2228–2234. [CrossRef] [PubMed]
137. Hirakawa, T.; Kamat, P.V. Charge separation and catalytic activity of Ag@TiO_2 core-shell composite clusters under UV-irradiation. *J. Am. Chem. Soc.* **2005**, *127*, 3928–3934. [CrossRef] [PubMed]
138. Luth, H. *Solid Surfaces, Interfaces, and Films*; Springer: Berlin, Germany, 2001.
139. Kozlov, D.A.; Lebedev, V.A.; Polyakov, A.Y.; Khazova, K.M.; Garshev, A.V. The microstructure effect on the Au/TiO_2 and Ag/TiO_2 nanocomposites photocatalytic activity. *Nanosyst. Phys. Chem. Math.* **2018**, *9*, 266–278. [CrossRef]
140. Leong, K.H.; Chu, H.Y.; Ibrahim, S.; Saravanan, P. Palladium nanoparticles anchored to anatase TiO_2 for enhanced surface plasmon resonance-stimulated, visible-light-driven photocatalytic activity. *Beilstein J. Nanotechnol.* **2015**, *6*, 428–437. [CrossRef]
141. Tapin, B.; Epron, F.; Especel, C.; Ly, B.K.; Pinel, C.; Besson, M. Study of monometallic Pd/TiO_2 catalysts for the hydrogenation of succinic acid in aqueous phase. *ACS Catal.* **2013**, *3*, 2327–2335. [CrossRef]
142. Keihan, A.H.; Rasoulnezhad, H.; Mohammadgholi, A.; Sajjadi, A.; Hosseinzadeh, R.; Farhadian, M.; Hosseinzadeh, G. Pd nanoparticle loaded TiO_2 semiconductor for photocatalytic degradation of Paraoxon pesticide under visible-light irradiation. *J. Mater. Sci. Mater. Electron.* **2017**, *28*, 16718–16727. [CrossRef]
143. Pham, M.H.; Dinh, C.T.; Vuong, G.T.; Do, T.O. General route toward hollow photocatalyst with two cocatalysts separated on two surface sides for hydrogen generation. *Phys. Chem. Chem. Phys.* **2014**, *16*, 5937–5941. [CrossRef]
144. Galinska, A.; Walendziewski, J. Photocatalytic water splitting over Pt-TiO_2 in the presence of sacrificial reagents. *Energy Fuels* **2005**, *19*, 1143–1147. [CrossRef]
145. Nguyen, C.C.; Nguyen, D.T.; Do, T.O. A novel route to synthesize C/Pt/TiO_2 phase tunable anatase-rutile TiO_2 for efficient sunlight-driven photocatalytic applications. *Appl. Catal. B Environ.* **2018**, *226*, 46–52. [CrossRef]
146. Liu, K.; Litke, A.; Su, Y.; van Campenhout, B.G.; Pidko, E.A.; Hensen, E.J.M. Photocatalytic decarboxylation of lactic acid by Pt/TiO_2. *Chem. Commun.* **2016**, *52*, 11634–11637. [CrossRef] [PubMed]
147. Fang, L.; You, L.; Liu, J. Ferroelectrics in Photocatalysis. In *Ferroelectric Materials for Energy Applications*; Huang, H., Scott, J.F., Eds.; Wiley-VCH Verlag GmbH & Co. KGaA: Weinheim, Germany, 2019.
148. Cui, Y.; Briscoe, J.; Dunn, S. Effect of ferroelectricity on solar-light-driven photocatalytic activity of $BaTiO_3$-influence on the carrier separation and stern layer formation. *Chem. Mater.* **2013**, *25*, 4215–4223. [CrossRef]
149. Jones, P.M.; Dunn, S. Photo-reduction of silver salts on highly heterogeneous lead zirconate titanate. *Nanotechnology* **2007**, *18*, 185702. [CrossRef]
150. Park, S.; Lee, C.W.; Kang, M.G.; Kim, S.; Kim, H.J.; Kwon, J.E.; Park, S.Y.; Kang, C.Y.; Hong, K.S.; Nam, K.T. A ferroelectric photocatalyst for enhancing hydrogen evolution: Polarized particulate suspension. *Phys. Chem. Chem. Phys.* **2014**, *16*, 10408–10413. [CrossRef] [PubMed]

151. Li, L.; Salvador, P.A.; Rohrer, G.S. Photocatalysts with internal electric fields. *Nanoscale* **2014**, *6*, 24–42. [CrossRef] [PubMed]
152. Huang, H.; Tu, S.; Du, X.; Zhang, Y. Ferroelectric spontaneous polarization steering charge carriers migration for promoting photocatalysis and molecular oxygen activation. *J. Colloid Interface Sci.* **2018**, *509*, 113–122. [CrossRef]
153. Cui, Y.; Briscoe, J.; Wang, Y.; Tarakina, N.V.; Dunn, S. Enhanced photocatalytic activity of heterostructured ferroelectric $BaTiO_3$/α-Fe_2O_3 and the significance of interface morphology control. *ACS Appl. Mater. Interfaces* **2017**, *9*, 24518–24526. [CrossRef]
154. Fu, Q.; Wang, X.; Li, C.; Sui, Y.; Han, Y.; Lv, Z.; Song, B.; Xu, P. Enhanced photocatalytic activity on polarized ferroelectric $KNbO_3$. *RSC Adv.* **2016**, *6*, 108883–108887. [CrossRef]
155. Al-keisy, A.; Ren, L.; Cui, D.; Xu, Z.; Xu, X.; Su, X.; Hao, W.; Doua, S.X.; Du, Y. A ferroelectric photocatalyst Ag10Si4O13 with visible-light photooxidation properties. *J. Mater. Chem. A* **2016**, *4*, 10992–10999. [CrossRef]
156. Sakar, M.; Balakumar, S.; Saravanan, P.; Bharathkumar, S. Compliments of confinements: Substitution and dimension induced magnetic origin and band-bending mediated photocatalytic enhancements in $Bi_{1-x}Dy_xFeO_3$ particulate and fiber nanostructures. *Nanoscale* **2015**, *7*, 10667–10679. [CrossRef] [PubMed]
157. Sakar, M.; Balakumar, S.; Saravanan, P.; Bharathkumar, S. Particulates vs. fibers: Dimension featured magnetic and visible light driven photocatalytic properties of Sc modified multiferroic bismuth ferrite nanostructures. *Nanoscale* **2016**, *8*, 1147–1160. [CrossRef] [PubMed]
158. Sakar, M.; Balakumar, S.; Bhaumik, I.; Gupta, P.K.; Jaisankar, S.N. Nanostructured $Bi_{(1-x)}Gd_{(x)}FeO_3$-A multiferroic photocatalyst on its sunlight driven photocatalytic activity. *RSC Adv.* **2014**, *4*, 16871–16878.
159. Li, R.; Li, Q.; Zong, L.; Wang, X.; Yang, J. $BaTiO_3$/TiO_2 heterostructure nanotube arrays for improved photoelectrochemical and photocatalytic activity. *Electrochim. Acta* **2013**, *91*, 30–35. [CrossRef]
160. Küçük, O.; Teber, S.; Kaya, I.C.; Akyildiz, H.; Kalem, V. Photocatalytic activity and dielectric properties of hydrothermally derived tetragonal $BaTiO_3$ nanoparticles using TiO_2 nanofibers. *J. Alloys Compd.* **2018**, *765*, 82–91. [CrossRef]
161. Li, Q.; Li, R.; Zong, L.; He, J.; Wang, X.; Yang, J. Photoelectrochemical and photocatalytic properties of Ag-loaded $BaTiO_3$/TiO_2 heterostructure nanotube arrays. *Int. J. Hydrog. Energy* **2013**, *38*, 12977–12983. [CrossRef]
162. Zhang, Y.; Salvador, P.A.; Rohrer, G.S. Ferroelectric-enhanced photocatalysis with TiO_2/$BiFeO_3$. In *Energy Technology 2014*; Wang, C., de Bakker, J., Belt, C.K., Jha, A., Neelameggham, N.R., Pati, S., Prentice, L.H., Tranell, G., Brinkman, K.S., Eds.; The Minerals, Metals & Materials Society: Pittsburgh, PA, USA, 2014.
163. Li, S.; Lin, Y.H.; Zhang, B.P.; Li, J.F.; Nan, C.W. $BiFeO_3$/TiO_2 core-shell structured nanocomposites as visible-active photocatalysts and their optical response mechanism. *J. Appl. Phys.* **2009**, *105*, 054310. [CrossRef]
164. Liu, G.; Ma, L.; Yin, L.C.; Wan, G.; Zhu, H.; Zhen, C.; Yang, Y.; Liang, Y.; Tan, J.; Cheng, H.M. Selective chemical epitaxial growth of TiO_2 islands on ferroelectric $PbTiO_3$ crystals to boost photocatalytic activity. *Joule* **2018**, *2*, 1–13. [CrossRef]
165. Leary, R.; Westwood, A. Carbonaceous nanomaterials for the enhancement of TiO_2 photocatalysis. *Carbon* **2011**, *49*, 741–772. [CrossRef]
166. Khalid, N.R.; Majid, A.; Tahir, M.B.; Niaz, N.A.; Khalid, S. Carbonaceous-TiO_2 nanomaterials for photocatalytic degradation of pollutants: A review. *Ceram. Int.* **2017**, *43*, 14552–14571. [CrossRef]
167. Sakthivel, S.; Kisch, H. Daylight photocatalysis by carbon-modified titanium dioxide. *Angew. Chem. Int. Ed.* **2003**, *42*, 4908–4911. [CrossRef] [PubMed]
168. Yu, H.; Zhao, Y.; Zhou, C.; Shang, L.; Peng, Y.; Cao, Y.; Wu, L.Z.; Tunga, C.H.; Zhang, T. Carbon quantum dots/TiO_2 composites for efficient photocatalytic hydrogen evolution. *J. Mater. Chem. A* **2014**, *2*, 3344–3351. [CrossRef]
169. Yu, X.; Liu, J.; Yu, Y.; Zuo, S.; Li, S. Preparation and visible light photocatalytic activity of carbon quantum dots/TiO_2 nanosheet composites. *Carbon* **2014**, *68*, 718–724. [CrossRef]
170. Sathish Kumar, M.; Yamini Yasoda, K.; Kumaresan, D.; Kothurkar, N.K.; Batabyal, S.K. TiO_2-carbon quantum dots (CQD) nanohybrid: Enhanced photocatalytic activity. *Mater. Res. Express* **2018**, *5*, 075502. [CrossRef]
171. Ren, Y.; Dong, Y.; Feng, Y.; Xu, J. Compositing two-dimensional materials with TiO_2 for photocatalysis. *Catalysts* **2018**, *8*, 590. [CrossRef]

172. Baca, M.; Kukułka, W.; Cendrowski, K.; Mijowska, E.; Kaleńczuk, R.J.; Zielińska, B. Graphitic carbon nitride and titanium dioxide modified with 1 D and 2 D carbon structures for photocatalysis. *ChemSusChem* **2019**, *12*, 612–620. [CrossRef] [PubMed]
173. Olowoyo, J.O.; Kumar, M.; Jain, S.L.; Babalola, J.O.; Vorontsov, A.V.; Kumar, U. Insights into reinforced photocatalytic activity of the CNT-TiO_2 nanocomposite for co2 reduction and water splitting. *J. Phys. Chem. C* **2019**, *123*, 367–378. [CrossRef]
174. Shaban, M.; Ashraf, A.M.; Abukhadra, M.R. TiO_2 nanoribbons/carbon nanotubes composite with enhanced photocatalytic activity; fabrication, characterization, and application. *Sci. Rep.* **2018**, *8*, 781. [CrossRef]
175. Li, X.; Lin, H.; Chen, X.; Niu, H.; Zhang, T.; Liua, J.; Qu, F. Fabrication of TiO_2/porous carbon nanofibers with superior visible photocatalytic activity. *New J. Chem.* **2015**, *39*, 7863–7872. [CrossRef]
176. Kim, S.; Lim, S.K. Preparation of TiO_2-embedded carbon nanofibers and their photocatalytic activity in the oxidation of gaseous acetaldehyde. *Appl. Catal. B Environ.* **2008**, *84*, 16–20. [CrossRef]
177. Cao, L.; Sahu, S.; Anilkumar, P.; Bunker, C.E.; Xu, J.; Shiral Fernando, K.A.; Wang, P.; Guliants, E.A.; Tackett, K.N.; Sun, Y.P. Carbon nanoparticles as visible-light photocatalysts for efficient CO_2 conversion and beyond. *J. Am. Chem. Soc.* **2011**, *133*, 4754–4757. [CrossRef] [PubMed]
178. Zhong, J.; Chen, F.; Zhang, J. Carbon-deposited TiO_2: Synthesis, characterization, and visible photocatalytic performance. *J. Phys. Chem. C* **2010**, *114*, 933–939. [CrossRef]
179. Zhang, W.D.; Bin Xu, B.; Jiang, L.C. Functional hybrid materials based on carbon nanotubes and metal oxides. *J. Mater. Chem.* **2010**, *20*, 6383–6391. [CrossRef]
180. Yu, J.; Wang, S.; Lowa, J.; Xiao, W. Enhanced photocatalytic performance of direct Z-scheme g-C_3N_4-TiO_2 photocatalysts for the decomposition of formaldehyde in air. *Phys. Chem. Chem. Phys.* **2013**, *15*, 16883–16890. [CrossRef] [PubMed]
181. Tan, L.L.; Ong, W.J.; Chai, S.P.; Mohamed, A.R. Reduced graphene oxide-TiO_2 nanocomposite as a promising visible-light-active photocatalyst for the conversion of carbon dioxide. *Nanoscale Res. Lett.* **2013**, *8*, 465. [CrossRef] [PubMed]
182. Tan, L.; Chai, S.; Mohamed, A.R. Synthesis and applications of graphene-based TiO_2 photocatalysts. *ChemSusChem* **2012**, *5*, 1868–1882. [CrossRef] [PubMed]
183. Nasr, M.; Balme, S.; Eid, C.; Habchi, R.; Miele, P.; Bechelany, M. Enhanced visible-light photocatalytic performance of electrospun rGO/TiO_2 composite nanofibers. *J. Phys. Chem. C* **2017**, *121*, 261–269. [CrossRef]
184. Pan, X.; Zhao, Y.; Liu, S.; Korzeniewski, C.L.; Wang, S.; Fan, Z. Comparing graphene-TiO_2 nanowire and graphene-TiO_2 nanoparticle composite photocatalysts. *ACS Appl. Mater. Interfaces* **2012**, *4*, 3944–3950. [CrossRef] [PubMed]
185. Yu, H.; Xiao, P.; Tian, J.; Wang, F.; Yu, J. Phenylamine-functionalized rGO/TiO_2 photocatalysts: Spatially separated adsorption sites and tunable photocatalytic selectivity. *ACS Appl. Mater. Interfaces* **2016**, *8*, 29470–29477. [CrossRef] [PubMed]
186. Luo, B.; Liu, G.; Wang, L. Recent advances in 2D materials for photocatalysis. *Nanoscale* **2016**, *8*, 6904–6920. [CrossRef] [PubMed]
187. Singh, A.K.; Mathew, K.; Zhuang, H.L.; Hennig, R.G. Computational screening of 2D materials for photocatalysis. *J. Phys. Chem. Lett.* **2015**, *6*, 1087–1098. [CrossRef] [PubMed]
188. Zhang, C.; Huang, H.; Ni, X.; Zhou, Y.; Kang, L.; Jiang, W.; Chen, H.; Zhong, J.; Liu, F. Band gap reduction in van der Waals layered 2D materials via a de-charge transfer mechanism. *Nanoscale* **2018**, *10*, 16759–16764. [CrossRef] [PubMed]
189. Ida, S.; Ishihara, T. Recent progress in two-dimensional oxide photocatalysts for water splitting. *J. Phys. Chem. Lett.* **2014**, *5*, 2533–2542. [CrossRef] [PubMed]
190. Nguyen, C.C.; Vu, N.N.; Chabot, S.; Kaliaguine, S.; Do, T.O. Role of C_xN_y-triazine in photocatalysis for efficient hydrogen generation and organic pollutant degradation under solar light irradiation. *Solar RRL* **2017**, *1*, 1700012. [CrossRef]
191. Haque, F.; Daeneke, T.; Kalantar-zadeh, K.; Ou, J.Z. Two-dimensional transition metal oxide and chalcogenide-based photocatalysts. *Nano-Micro Lett.* **2018**, *10*, 23. [CrossRef] [PubMed]
192. Guo, L.; Yang, Z.; Marcus, K.; Li, Z.; Luo, B.; Zhou, L.; Wang, X.; Du, Y.; Yang, Y. MoS_2/TiO_2 heterostructures as nonmetal plasmonic photocatalysts for highly efficient hydrogen evolution. *Energy Environ. Sci.* **2018**, *11*, 106–114. [CrossRef]

193. Sun, Y.; Lin, H.; Wang, C.; Wu, Q.; Wang, X.; Yang, M. Morphology-controlled synthesis of TiO_2/MoS_2 nanocomposites with enhanced visible-light photocatalytic activity. *Inorg. Chem. Front.* **2018**, *5*, 145–152. [CrossRef]
194. Dong, Y.; Chen, S.Y.; Lu, Y.; Xiao, Y.X.; Hu, J.; Wu, S.M.; Deng, Z.; Tian, G.; Chang, G.G.; Li, J.; et al. Hierarchical MoS_2@TiO_2 heterojunctions for enhanced photocatalytic performance and electrocatalytic hydrogen evolution. *Chem. Asian J.* **2018**, *13*, 1609. [CrossRef]
195. Zhang, W.; Xiao, X.; Zheng, L.; Wan, C. Fabrication of TiO_2/MoS_2 composite photocatalyst and its photocatalytic mechanism for degradation of methyl orange under visible light. *Can. J. Chem. Eng.* **2015**, *93*, 1594–1602. [CrossRef]
196. Zhao, F.; Rong, Y.; Wan, J.; Hu, Z.; Peng, Z.; Wang, B. MoS_2 quantum dots@TiO_2 nanotube composites with enhanced photoexcited charges separation and high-efficiency visible-light driven photocatalysis. *Nanotechnology* **2018**, *29*, 105403. [CrossRef] [PubMed]
197. Liu, X.; Xing, Z.; Zhang, H.; Wang, W.; Zhang, Y.; Li, Z.; Wu, X.; Yu, X.; Zhou, W. Fabrication of 3D mesoporous black $TiO_2/MoS_2/TiO_2$ nanosheets for visible-light-driven photocatalysis. *ChemSusChem* **2016**, *9*, 1118–1124. [CrossRef] [PubMed]
198. Zhu, Y.; Ling, Q.; Liu, Y.; Wang, H.; Zhu, Y. Photocatalytic H_2 evolution on MoS_2-TiO_2 catalysts synthesized via mechanochemistry. *Phys. Chem. Chem. Phys.* **2015**, *17*, 933–940. [CrossRef] [PubMed]
199. Liu, X.; Xing, Z.; Zhang, Y.; Li, Z.; Wu, X.; Tan, S.; Yu, X.; Zhu, Q.; Zhou, W. Fabrication of 3D flower-like black N-TiO_{2-x}@MoS_2 for unprecedented-high visible-light-driven photocatalytic performance. *Appl. Catal. B Environ.* **2017**, *201*, 119–127. [CrossRef]
200. Zhang, J.; Zhang, L.; Ma, X.; Ji, Z. A study of constructing heterojunction between two-dimensional transition metal sulfides (MoS_2 and WS_2) and (101),(001) faces of TiO_2. *Appl. Surf. Sci.* **2018**, *430*, 424–437. [CrossRef]
201. Chu, H.; Lei, W.; Liua, X.; Lib, J.; Zheng, W.; Zhu, G.; Li, C.; Pan, L.; Sun, C. Synergetic effect of TiO_2 as co-catalyst for enhanced visible light photocatalytic reduction of Cr (VI) on $MoSe_2$. *Appl. Catal. A Gen.* **2016**, *521*, 19–25. [CrossRef]
202. Shen, Y.; Ren, X.; Xu, G.; Huang, Z.; Qi, X. Mixed-dimensional TiO_2 nanoparticles with $MoSe_2$ nanosheets for photochemical hydrogen generation. *J. Mater. Sci. Mater. Electron.* **2017**, *28*, 2023–2028. [CrossRef]
203. Zheng, X.; Yang, L.; Li, Y.; Yang, L.; Luo, S. Direct Z-scheme $MoSe_2$ decorating TiO_2 nanotube arrays photocatalyst for water decontamination. *Electrochim. Acta* **2019**, *298*, 663–669. [CrossRef]
204. Cao, S.; Liu, T.; Hussain, S.; Zeng, W.; Peng, X.; Pan, F. Hydrothermal synthesis, characterization and optical absorption property of nanoscale WS_2/TiO_2 composites. *Phys. E Low-Dimens. Syst. Nanostruct.* **2015**, *68*, 171–175. [CrossRef]
205. Ren, X.; Qiao, H.; Huang, Z.; Tang, P.; Liu, S.; Luo, S.; Yao, H.; Qi, X.; Zhong, J. Investigating the photocurrent generation and optoelectronic responsivity of WS_2-TiO_2 heterostructure. *Optics Commun.* **2018**, *406*, 118–123. [CrossRef]
206. Cho, E.C.; Chang-Jian, C.W.; Zheng, J.H.; Huang, J.H.; Lee, K.C.; Ho, B.C.; Hsiao, Y.S. Microwave-assisted synthesis of TiO_2/WS_2 heterojunctions with enhanced photocatalytic activity. *J. Taiwan Ins. Chem. Eng.* **2018**, *91*, 489–498. [CrossRef]
207. Wu, Y.; Liu, Z.; Li, Y.; Chen, J.; Zhu, X.; Na, P. Construction of 2D-2D TiO_2 nanosheet/layered WS_2 heterojunctions with enhanced visible-light-responsive photocatalytic activity. *Chin. J. Catal.* **2019**, *40*, 60–69. [CrossRef]
208. Wu, Y.; Liu, Z.; Li, Y.; Chen, J.; Zhu, X.; Na, P. WS_2 nanodots-modified TiO_2 nanotubes to enhance visible-light photocatalytic activity. *Mater. Lett.* **2019**, *240*, 47–50. [CrossRef]
209. Ho, W.; Yu, J.C.; Lin, J.; Yu, J.; Li, P. Preparation and photocatalytic behavior of MoS_2 and WS_2 nanocluster sensitized TiO_2. *Langmuir* **2004**, *20*, 5865–5869. [CrossRef] [PubMed]
210. Dowla Biswas, M.R.U.; Ali, A.; Cho, K.Y.; Oh, W.C. Novel synthesis of WSe_2-Graphene-TiO_2 ternary nanocomposite via ultrasonic technics for high photocatalytic reduction of CO_2 into CH_3OH. *Ultrason. Sonochem.* **2018**, *42*, 738–746. [CrossRef]
211. Nasalevich, M.A.; van der Veen, M.; Kapteijn, F.; Gascon, J. Metal-organic frameworks as heterogeneous photocatalysts: Advantages and challenges. *CrystEngComm* **2014**, *16*, 4919–4926. [CrossRef]
212. Zhang, T.; Lin, W. Metal-organic frameworks for artificial photosynthesis and photocatalysis. *Chem. Soc. Rev.* **2014**, *43*, 5982–5993. [CrossRef]

213. Li, Y.; Xu, H.; Ouyang, S.; Ye, J. Metal-organic frameworks for photocatalysis. *Phys. Chem. Chem. Phys.* **2016**, *18*, 7563–7572. [CrossRef]
214. Dhakshinamoorthy, A.; Li, Z.; Garcia, H. Catalysis and photocatalysis by metal organic frameworks. *Chem. Soc. Rev.* **2018**, *47*, 8134–8172. [CrossRef]
215. Xiao, J.D.; Jiang, H.L. Metal-organic frameworks for photocatalysis and photothermal catalysis. *Acc. Chem. Res.* **2019**, *52*, 356–366. [CrossRef]
216. Qiu, J.; Zhang, X.; Feng, Y.; Zhang, X.; Wang, H.; Yao, J. Modified metal-organic frameworks as photocatalysts. *Appl. Catal. B Environ.* **2018**, *231*, 317–342. [CrossRef]
217. Yao, P.; Liu, H.; Wang, D.; Chen, J.; Li, G.; An, T. Enhanced visible-light photocatalytic activity to volatile organic compounds degradation and deactivation resistance mechanism of titania confined inside a metal-organic framework. *J. Colloid Interface Sci.* **2018**, *522*, 174–182. [CrossRef] [PubMed]
218. Crake, A.; Christoforidis, K.C.; Kafizas, A.; Zafeiratos, S.; Petit, C. CO_2 capture and photocatalytic reduction using bifunctional TiO_2/MOF nanocomposites under UV-vis irradiation. *Appl. Catal. B Environ.* **2017**, *210*, 131–140. [CrossRef]
219. Ling, L.; Wang, Y.; Zhang, W.; Ge, Z.; Duan, W.; Liu, B. Preparation of a novel ternary composite of TiO_2/UiO-66-NH_2/Graphene Oxide with enhanced photocatalytic activities. *Catal. Lett.* **2018**, *148*, 1978–1984. [CrossRef]
220. Cardoso, J.C.; Stulp, S.; de Brito, J.F.; Flor, J.B.S.; Frem, R.C.G.; Zanoni, M.V.B. MOFs based on ZIF-8 deposited on TiO_2 nanotubes increase the surface adsorption of CO_2 and its photoelectrocatalytic reduction to alcohols in aqueous media. *Appl. Catal. B Environ.* **2018**, *225*, 563–573. [CrossRef]
221. Wang, M.; Wang, D.; Li, Z. Self-assembly of CPO-27-Mg/TiO_2 nanocomposite with enhanced performance for photocatalytic CO_2 reduction. *Appl. Catal. B Environ.* **2016**, *183*, 47–52. [CrossRef]
222. Zhang, B.; Zhang, J.; Tan, X.; Shao, D.; Shi, J.; Zheng, L.; Zhang, J.; Yang, G.; Han, B. MIL-125-NH_2@TiO_2 Core-shell particles produced by a post-solvothermal route for high-performance photocatalytic H_2 production. *ACS Appl. Mater. Interfaces* **2018**, *10*, 16418–16423. [CrossRef]
223. Zhao, C.W.; Li, Y.A.; Wang, X.R.; Chen, G.J.; Liu, Q.K.; Ma, J.P.; Dong, Y.B. Fabrication of Cd (II)-MOF-based ternary photocatalytic composite materials for H_2 production via gel-to-crystal approach. *Chem. Commun.* **2015**, *51*, 15906–15909. [CrossRef]
224. Li, X.; Pi, Y.; Hou, Q.; Yu, H.; Li, Z.; Li, Y.; Xiao, J. Amorphous TiO_2@NH_2-MIL-125(Ti) homologous MOF encapsulated heterostructures with enhanced photocatalytic activity. *Chem. Commun.* **2018**, *54*, 1917–1920. [CrossRef]
225. Xue, C.; Zhang, F.; Chang, Q.; Dong, Y.; Wang, Y.; Hu, S.; Yang, J. MIL-125 and NH_2-MIL-125 modified TiO_2 nanotube array as efficient photocatalysts for pollute degradation. *Chem. Lett.* **2018**, *47*, 711–714. [CrossRef]
226. Xing, M.; Fang, W.; Nasir, M.; Ma, Y.; Zhang, J.; Anpo, M. Self-doped Ti^{3+}-enhanced TiO_2 nanoparticles with a high-performance photocatalysis. *J. Catal.* **2013**, *297*, 236–243. [CrossRef]
227. Zhang, R.; Yang, Y.; Leng, S.; Wang, Q. Photocatalytic activity of Ti^{3+} self-doped dark TiO_2 ultrafine nanorods, grey SiO_2 nanotwin crystalline, and their composite under visible light. *Mater. Res. Express* **2018**, *5*, 045044. [CrossRef]
228. Liu, X.; Gao, S.; Xu, H.; Lou, Z.; Wang, W.; Huang, B.; Dai, Y. Green synthetic approach for Ti^{3+} self-doped TiO_{2-x} nanoparticles with efficient visible light photocatalytic activity. *Nanoscale* **2013**, *5*, 1870–1875. [CrossRef] [PubMed]
229. Hao, W.; Li, X.; Qin, L.; Han, S.; Kang, S.Z. Facile preparation of Ti^{3+} self-doped TiO_2 nanoparticles and their dramatic visible photocatalytic activity for fast restoration of highly concentrated Cr (VI) effluent. *Catal. Sci. Technol.* **2019**, *9*, 2523–2531. [CrossRef]
230. Zheng, Z.; Huang, B.; Meng, X.; Wang, J.; Wang, S.; Lou, Z.; Wang, Z.; Qin, X.; Zhang, X.; Dai, Y. Metallic zinc-assisted synthesis of Ti^{3+} self-doped TiO_2 with tunable phase composition and visible-light photocatalytic activity. *Chem. Commun.* **2013**, *49*, 868–870. [CrossRef] [PubMed]
231. Naldoni, A.; Allieta, M.; Santangelo, S.; Marelli, M.; Fabbri, F.; Cappelli, S.; Bianchi, C.L.; Psaro, R.; Santo, V.D. Effect of nature and location of defects on bandgap narrowing in black TiO_2 nanoparticles. *J. Am. Chem. Soc.* **2012**, *134*, 7600–7603. [CrossRef] [PubMed]
232. Ullattil, S.G.; Narendranath, S.B.; Pillai, S.C.; Periyat, P. Black TiO_2 nanomaterials: A review of recent advances. *Chem. Eng. J.* **2018**, *343*, 708–736. [CrossRef]

233. Wang, B.; Shen, S.; Mao, S.S. Black TiO_2 for solar hydrogen conversion. *J. Materiomics* **2017**, *3*, 96–111. [CrossRef]
234. Chen, X.; Liu, L.; Huang, F. Black titanium dioxide (TiO_2) nanomaterials. *Chem. Soc. Rev.* **2015**, *44*, 1861–1885. [CrossRef]
235. Chen, X.B.; Liu, L.; Yu, P.Y.; Mao, S.S. Increasing solar absorption for photocatalysis with black hydrogenated titanium dioxide nanocrystals. *Science* **2011**, *331*, 746–750. [CrossRef]
236. Zhu, Q.; Peng, Y.; Lin, L.; Fan, C.M.; Gao, G.Q.; Wang, R.X.; Xu, A.W. Stable blue TiO_{2-x} nanoparticles for efficient visible light photocatalysts. *J. Mater. Chem. A* **2014**, *2*, 4429–4437. [CrossRef]
237. Wu, Q.; Huang, F.; Zhao, M.; Xu, J.; Zhou, J.; Wang, Y. Ultra-small yellow defective TiO_2 nanoparticles for co-catalyst free photocatalytic hydrogen production. *Nano Energy* **2016**, *24*, 63–71. [CrossRef]
238. Liu, G.; Yin, L.C.; Wang, J.; Niu, P.; Zhen, C.; Xie, Y.; Cheng, H.M. A red anatase TiO_2 photocatalyst for solar energy conversion. *Energy Environ. Sci.* **2012**, *5*, 9603–9610. [CrossRef]
239. Ren, R.; Wen, Z.; Cui, S.; Hou, Y.; Guo, X.; Chen, J. Controllable synthesis and tunable photocatalytic properties of Ti^{3+}-doped TiO_2. *Sci. Rep.* **2015**, *5*, 10714. [CrossRef] [PubMed]
240. Fan, C.; Chen, C.; Wang, J.; Fu, X.; Ren, Z.; Qian, G.; Wang, Z. Enhanced photocatalytic activity of hydroxylated and N-doped anatase derived from amorphous hydrate. *J. Mater. Chem. A* **2014**, *2*, 16242–16249. [CrossRef]